Wideband, Wide-Scan Planar Connected Slot Array Enhanced with Artificial Dielectrics

MASTER OF SCIENCE THESIS

For the degree of Master of Science in Electrical Engineering at Delft University of Technology

Harshitha Thippur Shivamurthy

10th September, 2014

TU Delft Delft University of Technology

Wideband, Wide-Scan Planar Connected Slot Array Enhanced with Artificial Dielectrics

Harshitha Thippur Shivamurthy

supervised by:

prof. dr. ing. A. Neto

co-supervised by:

dr. Daniele Cavallo

Terahertz Sensing Group
Faculty of Electrical Engineering, Mathematics and Computer Science
Delft University of Technology

DELFT UNIVERSITY OF TECHNOLOGY
DEPARTMENT OF
TELECOMMUNICATION

The undersigned hereby certify that they have read and recommend to the Faculty of Electrical Engineering, Mathematics and Computer Science for acceptance a thesis entitled **"Wideband, wide-scan planar connected slot array enhanced with artificial dielectrics"** by **Harshitha Thippur Shivamurthy** in partial fulfillment of the requirements for the degree of Master of Science.

Dated: 10-09-2014

Chairman:

prof. dr. ing. A. Neto

Advisors:

prof. dr. ing. A. Neto

dr. Daniele Cavallo

Committee Members:

dr. N. Llombart Juan

dr. Marco Spirito

Contents

List of Figures

List of Tables

Acknowledgements

I would like to express my sincere gratitude to my supervisor prof. dr. ing. A. Neto for providing me with an opportunity to carry out my master thesis in his group. His belief in my learning and performance abilities has been very encouraging. Thank you for your support.

This work would not have come about without the immense support and guidance of dr. Daniele Cavallo. The help that he offers is commendable. I immensely appreciate the effort he put in reviewing my thesis and teaching every concept with great patience. He is an outstanding supervisor and a mentor. Thank you for everything.

I thank dr. Nuria Llombart for her constant support throughout my thesis. You are a true role model.

I am grateful to Waqas for his constant support throughout the duration of my thesis. The time he spent in making me understand various concepts is praiseworthy and his dedication to work is inspiring. He is exceptionally good in using autocad tools and matlab. Everything that I have learnt regarding the usage of these tools is solely because of him. Thank you very much.

I would like to thank Beatriz, Maria, Alessandro, Erio and Ozan for being such amazing colleagues, who have always encouraged and appreciated my work.

A very special thank you to Vishu, Manju, Phani, Arun, Adi and Abhi for their consistent support throughout the two years of my stay in Netherlands. You guys are and will always be very dear to me.

Madhuri, thank you for supporting me in all my endeavors. You are the sister I never had.

I dedicate this thesis to my parents, Nalina and Shivamurthy, and my

brother, Hitesh. Thank you for being my strength and I will always be indebted to you for your unwavering support.

Abstract

In this thesis, the design of planar connected array of slots loaded with artificial dielectric layers (ADLs) is proposed to achieve wideband and wide-scan capabilities. ADLs are used due to the potential advantage of low surface-wave loss and high radiation efficiency. Whereas, the connected array of slots avoid the implementation of baluns which add-on to complexity of the structure. Using ADL on top of the connected array of slots help in placing the backing reflector very close to the array plane, thereby making it possible to realize the vertical lines using via-hole technology. The planarity of the array results in significant reduction in fabrication costs and manufacturing complexity. Subsequently, an analytical tool is presented that can evaluate the performance of a single-pol array loaded with ADLs with minimal resources and high precision with respect to a commercial EM solver. The single-pol designed in then extended to dual-pol configuration that has a -10 dB matching from 7 to 13 GHz for scanning upto 50° in all azimuthal planes. The maximum cross-pol level of -10 dB is achieved for scanning in the diagonal plane. The radiation efficiency of the array is $> 95\%$.

Chapter 1

Introduction

1.1 Background

Wideband, wide-scanning arrays have been receiving great attention in the last few decades for both military and commercial applications, such as satellite communications, multi-functional radars, radio astronomy, etc.

On military platforms such as ships or airplanes, the high number of co-existing systems that support various functionalities (e.g. tracking, surveillance or discrimination), has lead to an increasing interest in wideband, wide-scan arrays. Since space and weight is a major constraint in these scenarios, having a different aperture for each function is often not a feasible option. It is then required to combine several systems in a single antenna aperture, which can simultaneously provide several functionalities. In some cases, these systems are also required to support communication services, which makes polarization purity an important aspect to be accounted for.

Also for satellite communication applications, a single wideband, wide-scan antenna array is advantageous for weight and space reduction. For example, recent activities have been proposed in [1], aiming at the investigation of wideband arrays for in-flight entertainment applications. This system requires to support two orthogonal polarizations, with low cross-polarization levels and wide-angle coverage.

Another important application that benefits from wideband, wide-scan arrays is radio astronomy. An ongoing project that requires large arrays with such characteristics is the Square Kilometer Array (SKA) [2, 3, 4]. The SKA

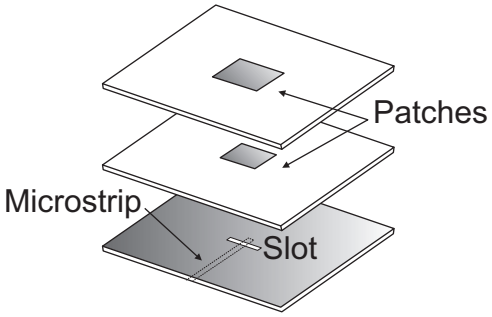

Figure 1.1: Stacked patches

is an international project aimed at building a very large radio telescope that will provide high sensitivity space observation.

1.1.1 State of the art

The most typical antenna solutions used in wideband wide-scanning arrays can be classified in three categories: stacked patches, tapered slot antennas, and connected array.

Stacked patches

Stacked patches have been shown to achieve about an octave bandwidth, for a linearly polarized array, capable to scan up to 45 degrees in all azimuthal planes [5]. However, the maximum possible bandwidth achievable with this solution is limited by the inherent resonant characteristic of the radiators. For this reason, the stacked patch element cannot be used for applications that require extremely large bandwidths.

Tapered slot antennas

Vivaldi antennas, which belong to the family of tapered slot antennas, are used extensively in applications such as radio astronomy, communication, remote sensing, etc., which require bandwidth in the order of a couple of octaves. These antennas [6, 7] have been shown to achieve larger bandwidth operation (multi-octave), over wide scan volume. Despite the good performance in terms of impedance matching, the large bandwidth come often at

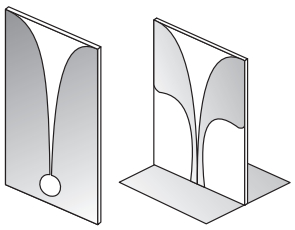

Figure 1.2: Tapered slot antennas

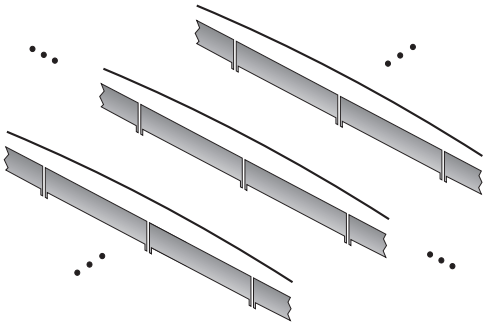

Figure 1.3: Connected arrays

the cost of degraded performance in terms of polarization purity, especially for scanning in diagonal planes [8];

Connected arrays

Another concept introduced more recently [9] is based on connected arrays. A connected array is an array of either slots or dipoles which are electrically connected to each other. They have the advantages of being broadband and, at the same time, having low cross polarization. Connected arrays are characterized by flat current distribution due to the electrical connection between the successive antenna elements, whereas resonant elements support sinusoidal (thus strongly frequency dependent) current distribution. Practically the bandwidth of a connected array is limited by the distance from the backing reflector, which is needed to ensure unidirectional radiation.

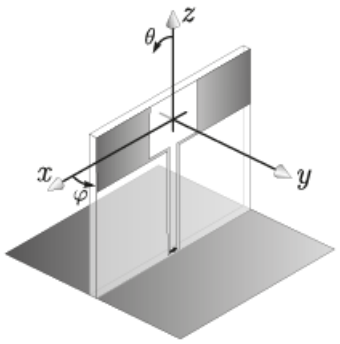

Figure 1.4: Vertical lines

1.1.2 Issues related to the assembly and manufacturing complexity

All phased arrays with wideband, wide-scan characteristics, which show stable performance and high-efficiency over the entire frequency band of operation, are characterized by a difficult three-dimensional assembly that renders the fabrication costly and complex.

Some of the state-of-the-art designs of Vivaldi and connected arrays that can be found in literature are shown in Fig. 1.1, 1.2 and 1.3 In these arrays, the typical complex egg-crate configuration is implemented, which consists of a set of vertical printed circuit boards (PCB's) arranged in a three-dimensional grid.

The reason for vertical PCB's is related to the need of the antenna to provide an unidirectional radiation. In Vivaldi array, a long vertical flaring is used in the element to increase the directivity. In connected array, a backing reflector is typically placed at about a quarter wavelength distance from the array plane, thus vertical feeding lines are needed to connect the elements to the feeds located below the ground plane. In both cases, long vertical feeding structures are essential to realized the unidirectional characteristics.

Vertical PCB's have to be used to realize such long lines which adds on to the assembly complexity. The vertical lines are so long that it is not possible to realize them using standard PCB via-hole technology, as shown in Fig. The vertical PCB realization does not allow for the choice of slot elements, which can be fed by unbalanced line, as opposed to dipole element, which

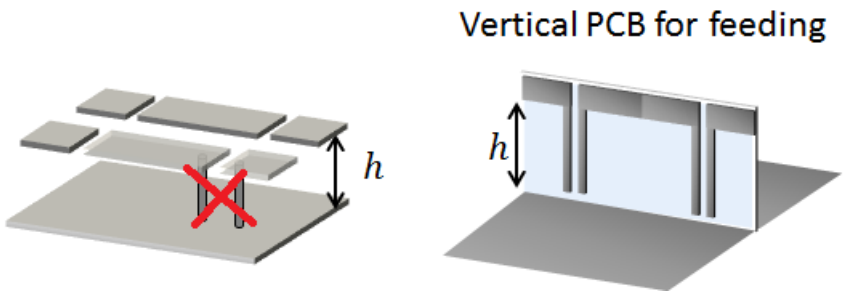

Figure 1.5: Vertical PCB

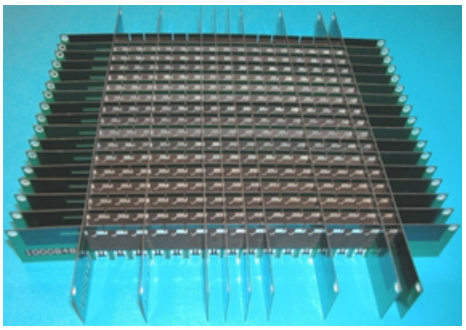

Figure 1.6: Complex assembly of vertical PCB's

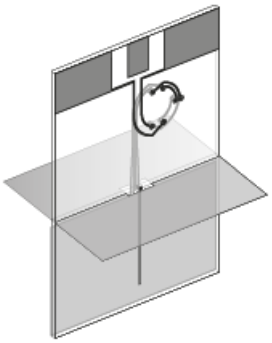

Figure 1.7: Complex assembly of vertical PCB's

require differential feeding lines and ad-hoc balun design. Such balun's are often the limiting factor for the bandwidth performance.

1.2 Solution proposed in this thesis

1.2.1 Objectives

The main objective of this thesis is to avoid the usage of vertical PCBs in the connected array design and to develop a completely planar structure. Such structure would be low-cost and easier to manufacture. Besides, connected slots are selected as radiating elements, to avoid the use of differential feed lines, which can support undesired common mode resonances. The aim is to design an array to have wide-scan and wideband capabilities with minimal cross polarization, which is especially important for communication applications.

1.2.2 Proposed solution

To achieve a structure with the above mentioned characteristics, a combination of connected array with artificial dielectric slabs is proposed in this thesis

Artificial dielectric layers are metallic inclusions in a dielectric host medium to enhance the permittivity of the medium by a required factor. The factor by which the permittivity of a medium can be varied depends on the physical dimensions of the metallic patches and their placements with reference to the other patch. Artificial dielectric layers have been used in the design to enhance the front-to-back ratio of the antenna and to minimize the excitation of the surface waves, ref [10].

The artificial dielectric allows to significantly reduce the distance between the array and the backing reflector, in such a way to permit the implementation of the element feed by means of standard via-hole technology. Consequently, a fully planar implementation of the array is enabled by the proposed solution.

1.2.3 Outline of the thesis

The thesis is organized into six chapters: Chapter 2 is on the connected array of slots and presents the analytical model used for representing the active input impedance of the array element, with and without the backing reflector. Chapter 3 reports on the analysis tools used for the design of

artificial dielectric layers. Chapter 4 introduces the design of the connected array of slots in the presence of the artificial dielectric layers and reports on the performance that can be achieved with this concept. In Chapter 5, single-pol and dual-pol prototype design is presented along with the feed network taking into account all the fabrication constraints. Last but not the least, chapter 6 derives the conclusions, highlighting the important concepts that were understood during the design and analysis period, along with the future work.

Chapter 2

Connected Arrays

2.1 Introduction

The concept of connected arrays was introduced by Hansen in [11], with the aim of increasing the bandwidth performance of dipole arrays. After their introduction, connected arrays have been extensively investigated and many designs have been presented in literature, for example in [12, 13, 14]. Connected array antennas are nowadays considered as one of the most promising solutions for wideband, low cross-pol, wide-scan applications, such as multi-function radars, electronic-warfare support measures (ESM) systems, Satcom and radioastronomy.

In standard narrow-band array designs, the objective is to keep the mutual coupling between the antenna elements low and to not alter the performance of each isolated element. In recent years, a new approach has been considered for the design of broadband arrays in which mutual coupling is intentionally introduced between the array elements. A simple way to enhance the coupling between neighboring elements is to electrically connect one to another. A connected array can be briefly described as an array of slots or dipoles which are electrically connected to each other. In this way, the array is no longer composed of separated resonant elements, but can be considered as a single antenna which is being fed periodically. The current distribution on resonant narrow-band dipoles is sinusoidal and frequency dependent, as shown in Fig. 2.1(b). Contrarily, connected arrays achieve wideband performance, due to the fact that the connections between neighboring elements

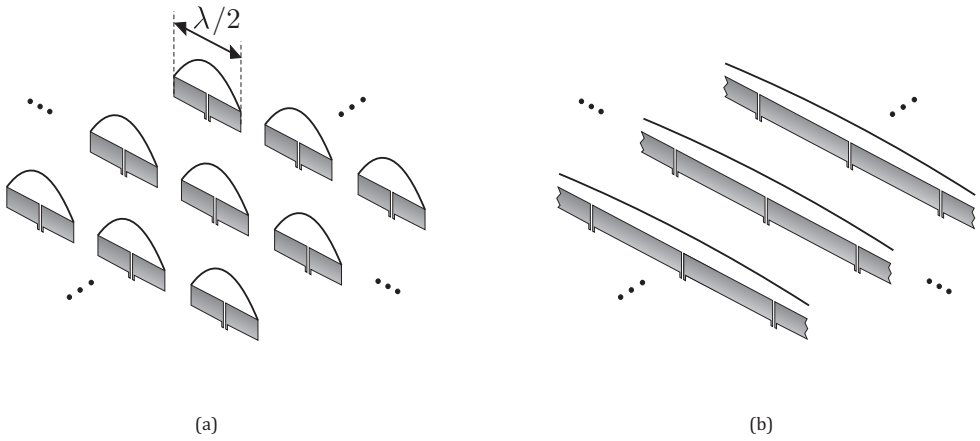

Figure 2.1: Current distribution on (a) resonant dipoles and (b) connected dipoles.

allow currents to remain nearly constant with frequency (see Fig. 2.1(a)). Thanks to the planarity of the radiators, the polarization purity is the most important advantages with respect to other existing technologies.

The performance of the connected arrays in terms of operational bandwidth, can be compared to that of the Vivaldi antennas. Theoretically infinite bandwidth can be achieved from the connected arrays radiating in free-space. However, in such configuration, there is 3 dB gain loss, as the array radiates equal power in the two half spaces. This efficiency loss can be avoided by adding a backing reflector, which ensures unidirectional radiation. The presence of such reflector introduces a dependence on the frequency, leading to a finite but still large bandwidth.

2.2 Array modeling

The analysis of connected arrays of slots and dipoles was extensively described in [9]. Figure 2.2 shows a two-dimensional connected array of slots in free space, where d_x and d_y are the periods of the unit cell, δ_s is the size of the feed gap and w_s is the width of the slots. The active input impedance of a unit cell is given by the following expression [15]:

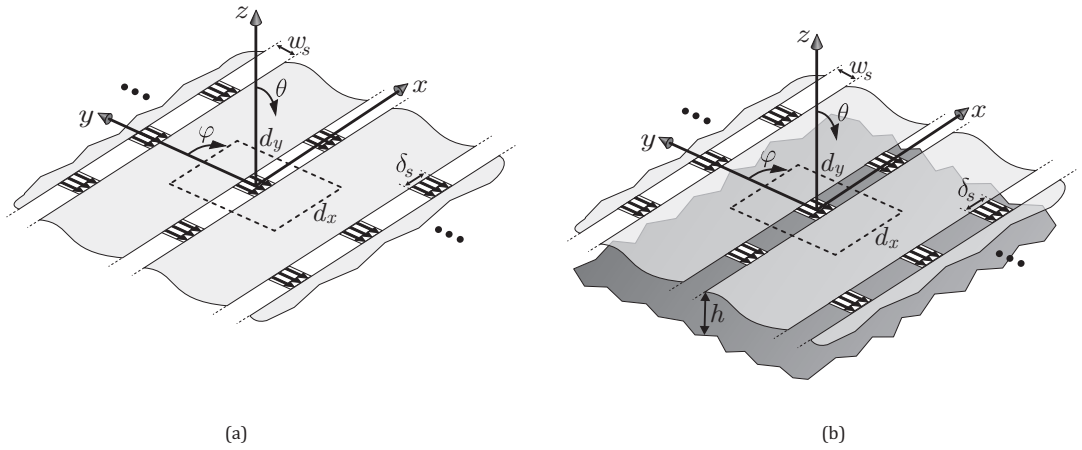

Figure 2.2: Connected array of slots in (a) free space and (b) with a backing reflector.

$$Z_{in} = \frac{1}{d_x} \sum_{m_x=-\infty}^{\infty} \frac{\mathrm{sinc}^2\left(k_{xm}\delta_s/2\right)}{D\left(k_{xm}\right)} \tag{2.1}$$

where the Floquet wavenumbers are defined as $k_{xm} = k_{x0} - \frac{2\pi m_x}{d_x}$ and $k_{ym} = k_{y0} - \frac{2\pi m_y}{d_y}$, m_x and m_y are the indexes of the Floquet modes; k_{x0} and k_{y0} represents the excitation wavenumbers in the longitudinal and transverse directions respectively and are given by $k_{x0} = k\sin\theta\cos\phi$, $k_{y0} = k\sin\theta\sin\phi$, with k being the propagation constant of medium. The orientation of the angles θ and ϕ with respect to the array plane is shown in Fig. 2.2.

The denominator function represents the connected slot array Green's function and is defined as

$$D\left(k_{xm}\right) = -\frac{1}{d_y} \sum_{m_y=-\infty}^{\infty} J_0\left(\frac{k_{ym}w_s}{2}\right) G_{xx}\left(k_{xm}, k_{ym}\right) \tag{2.2}$$

where J_0 is the Bessel function of zeroth order, which is the Fourier transform of the transverse magnetic current distribution across the slot. The function $G_{xx}\left(k_{xm}, k_{ym}\right)$ is the x-component of the spectral magnetic Green's function due to a magnetic dipole oriented along x:

$$G_{xx}\left(k_{xm}, k_{ym}, z\right) = -\frac{i_{TE}\left(z\right)k_{xm}^2 + i_{TM}\left(z\right)k_{ym}^2}{k_\rho^2} \tag{2.3}$$

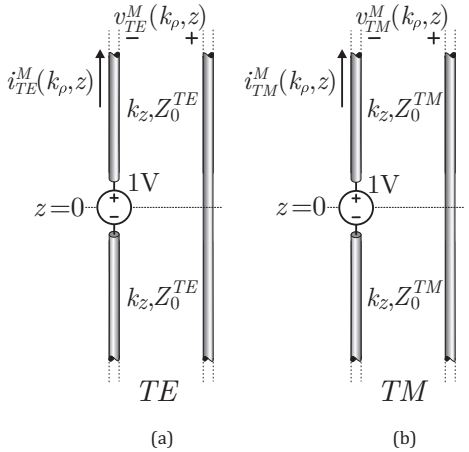

Figure 2.3: Equivalent transmission line of the spectral Green's function for (a) TE and (b) TM modes.

with $k_\rho = \sqrt{k_{xm}^2 + k_{ym}^2}$. The Green's function of any given stratification along z can be represented by an equivalent transverse electric (TE) and transverse magnetic (TM) transmission lines, with characteristic impedances $Z_{TE} = \eta \frac{k}{k_{zm}}$ and $Z_{TM} = \eta \frac{k_{zm}}{k}$, respectively ($\eta$ is intrinsic impedance of the medium). i_{TE} and i_{TM} represent the currents in these transmission lines.

With reference to the expressions in (2.1) and (2.2), the fundamental Floquet mode (for m_x=0 and m_y=0) denotes a homogeneous plane wave, whereas the higher order modes (when $m_x \neq 0$ and $m_y \neq 0$) refer to reactive, non-propagating energy, for electrically small array periods.

2.2.1 Equivalent transmission line Green's functions for different stratifications

In the case of connected arrays of slots in free space, the active input impedance of the array element can be calculated with the expressions (2.1) and (2.2), where the currents i_{TE} and i_{TM} in (2.3) are solutions of the equivalent transmission lines in Fig. 2.3. The two transmission lines for $z > 0$ and $z < 0$, represent the lower and upper half spaces above and below the array plane, respectively.

By implementing the analytical expressions given in (2.1), one can evaluate the frequency variation of the active impedance in the free space case.

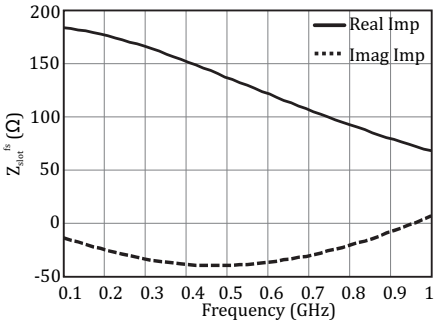

Figure 2.4: Frequency variation of the impedance of a connected array of slots suspended in free space. The periodicity of the unit cell are d_x=d_y=$0.5\lambda_0$, w_s=δ_s=$0.1\lambda_0$.

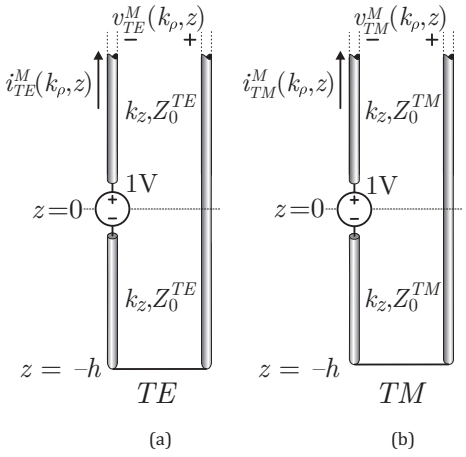

Figure 2.5: Equivalent transmission line of the spectral Green's function for (a) TE and (b) TM modes.

For example, Fig. 2.4 shows the active impedance for an array with dimensions d_x=d_y=$0.5\lambda_0$, and w_s=δ_s=$0.1\lambda_0$, with λ_0 being the wavelength at f_0.

The active input impedance of the connected array in the presence of a backing reflector can be derived in a similar way: by placing a metallic reflector at certain distance from the array plane the current and the voltage in the equivalent transmission line changes accordingly. The normalized current used in the evaluation of the Green's function for this stratification

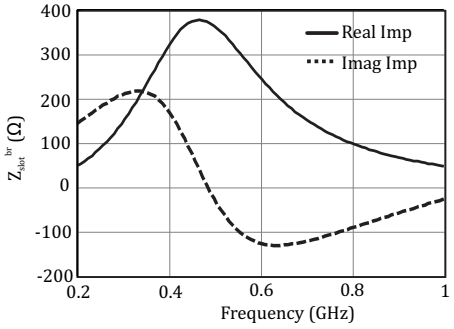

Figure 2.6: Frequency variation of the impedance of a connected array of slots in the presence of a backing reflector. The dimensions are d_x=d_y=$0.5\lambda_0$, w_s=δ_s=$0.1\lambda_0$, $h = 0.25\lambda_0$.

can be calculated by solving the transmission lines in Fig. 2.5. The active input impedance for an array characterized by d_x=d_y=$0.5\lambda_0$, w_s=δ_s=$0.1\lambda_0$ and $h = 0.25\lambda_0$ is shown in Fig. 2.6.

For a generic stratification composed by multiple dielectric slabs, the equivalent transmission line representation of the stratification includes multi-section transmission lines. Each dielectric slab is represented by a separate transmission line with length equal to the slab height, and characterized by characteristic impedance and propagation constant that depend on the material composing the slab.

Chapter 3

Artificial Dielectric Layers

3.1 Introduction

Artificial dielectrics (ADs) were introduced in late 1940's [16], to design light-weight and low-loss lens antennas. An AD consists of periodic metal inclusions in a host substrate to create an equivalent medium that enhances the dielectric constant of the host medium. This is because an incident wave undergoes a propagation delay when it encounters such metallic discontinuities in a homogeneous medium. A planar approach to realize ADs is to introduce metallic patches in a host medium, with the configuration shown in Fig. 3.1. These planar arrangements of the metallic inclusions are referred to as artificial dielectric layers (ADLs) and they are anisotropic in nature. The metallic patches are small in terms of the wavelength, thus non-resonant. Therefore, the resulting effective properties of the medium are characterized by a broadband frequency response. Thanks to the small dimensions of the metallic inclusions, the ohmic losses are typically very low for such structures.

Due to their planarity and enhanced dielectric properties, ADLs have been exploited for the design of compact on-chip passive components in commercial complementary metal-oxide semiconductors (CMOS) process in [17]. ADL-based solutions are also proposed for THz frequency domain spectroscopy and anti-reflection coating in [18, 19]. Some authors have used ADLs to reduce the volume occupancy of resonant Fabry-Perot antennas. In [20], a shield between the low-resistivity silicon substrate and the antenna is

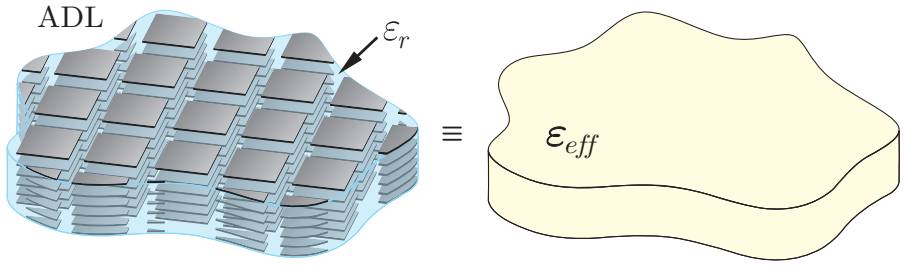

Figure 3.1: ADLs embedded in a host substrate is equivalent to a homogeneous medium.

realized using ADL.

Recently, ADL have been used to enhance the front-to-back ratio of an integrated antenna at 10 GHz [10]. In this contribution, the authors have exploited the ADL to realize an electrically thick superstrate with a physically thin dielectric slab. Due to the anisotropic properties of the ADL superstrate, almost no power is launched in surface waves, resulting in a very high radiation efficiency of the antenna.

A two-dimensional study of ADs under plane-wave incidence is presented in [21]. Recently, analytical spectral Green's functions of ADL are presented in [22, 23]. These works deal with the three-dimensional theoretical characterization of ADLs (see Fig. 3.1), under generic plane wave incidence, as well as for near-source excitation. In this chapter, this theory is exploited to design an analytical tool that is used to design connected arrays loaded with the ADL.

3.2 ADL analysis

ADLs are a cascade of periodic planar surfaces which are intended to realize a dielectric slab with the required permittivity. A single layer consists of an array of electrically small patches that are arranged in a rectangular grid. The scattering from both a single layer of patches and a multi-layer cascade was analyzed and formulated in [22, 23].

A single layer is depicted in Fig. 3.2 and is characterized by the array periods $d_{x,ADL}$ and $d_{y,ADL}$ along x and y, respectively, and width of the slots (i.e. gaps between adjacent patches) indicated as w_x and w_y. The slots

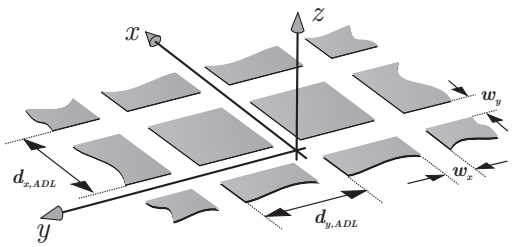

Figure 3.2: Single layer of periodic patches with periodicity $d_{x,ADL}$, $d_{y,ADL}$ and width of slot w_x, w_y.

are assumed to be electrically narrow.

Considering a plane wave incident on such layer with elevation and azimuth angle of incidence θ and ϕ, the equivalent impedance of the layer for TE and TM incidence is given by [22]

$$Z_{layer,TM} = \frac{-j}{B_s} \tag{3.1}$$

$$Z_{layer,TE} = \frac{-j}{B_s\left(1 - \frac{\sin^2\theta}{2}\right)} \tag{3.2}$$

where B_s is the self-susceptance (capacitance) of the slot, given by

$$B_s = \frac{2k_0}{\eta_0} \sum_{m_x \neq 0} \frac{|\mathrm{sinc}\,(k_{ym} w_x/2)\,|^2}{|k_{ym}|} \tag{3.3}$$

with $k_{ym} \approx \frac{2\pi m_y}{d_y}$. These expressions are accurate for unit cell dimensions that are smaller than a quarter wavelength. The equivalent impedances in (3.1) and (3.2) can be used to derive equivalent transmission line models for a plane wave impinging on a single layer. These models are shown in Fig. 3.3 and describe the reflection and transmission of the plane wave for transverse electric (TE) and transverse magnetic (TM) incidence. The TE and TM transmission lines would be coupled for array periods significantly larger than a quarter wavelength. However, as rigorously demonstrated in [22], for array periods smaller than a quarter wavelength, TE and TM mode are decoupled. In other words, a well sampled array of patches can scatter only TM waves under TM plane wave illumination and only TE waves under TE illumination. Another property of electrically dense arrays is that the

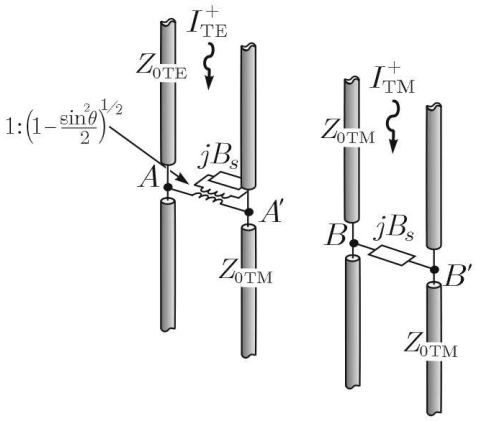

Figure 3.3: Equivalent transmission line model for a single ADL layer for TE and TM plane wave incidence.

scattering characteristics are independent of the azimuth angle of incidence ϕ.

For multi-layer ADL configurations, the inter-layer distance d_z is an additional parameter used to characterize the ADLs (refer to Fig. 3.2). For infinite number of layers embedded in a substrate, the slot susceptance is given by the following expression [23]:

$$B_{s\infty} = \frac{j2k_0}{\eta_0} \sum_{m_x \neq 0} \frac{|\mathrm{sinc}\,(k_{ym} w_x/2)\,|^2}{|k_{ym}|} \tan\left(\frac{k_{zm} d_z}{2}\right) \tag{3.4}$$

where $k_{zm} \approx -jk_{ym}$. The only modification with respect to the expression (3.3), valid for the single layer, is in the tangent term included in the higher-order Floquet modes.

However, when considering a finite number of ADL layers in a slab, the slot susceptance of the first and the last ADL layers can be described more accurately using a semi-infinite solution, to account for the truncation of the slab. It is given by the following expression [23]

$$B_{s,\mathrm{semi}\infty} = \frac{k_0}{\eta_0} \sum_{m_y \neq 0} \frac{|\mathrm{sinc}\,(k_{ym} w_x/2)\,|^2}{|k_{ym}|} \left(1 + j\tan\left(\frac{k_{zm} d_z}{2}\right)\right). \tag{3.5}$$

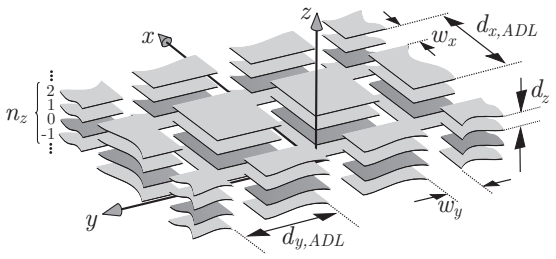

Figure 3.4: Multi-layer ADL configuration.

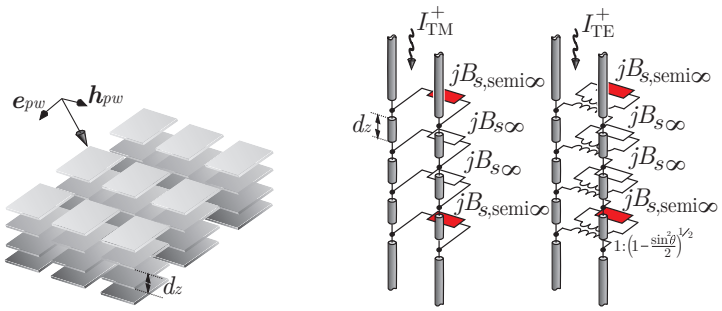

(a) (b)

Figure 3.5: (a) Finite height ADL slab and (b) equivalent transmission line model for TM and TE plane wave incidence.

Considering an ADL slab with four layers, the equivalent transmission line representation of the structure for TE and TM plane wave incidence is shown in Fig. 3.2.

3.3 Epsilon extraction

The entire ADL stratification can be represented as a cascade of two-port networks described by ABCD matrices, as shown in Fig. 3.6.

The ABCD matrix of an ADL layer and the inter-connecting transmission lines are represented as:

$$\begin{bmatrix} 1 & Z_{adl} \\ 0 & 1 \end{bmatrix} \tag{3.6}$$

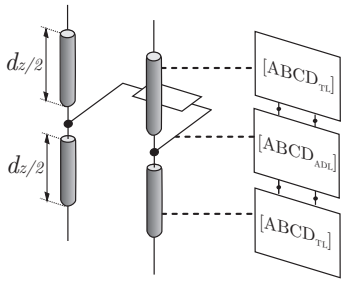

Figure 3.6: Cascade of ABCD blocks.

$$\begin{bmatrix} \cos\beta l & jZ\sin\beta l \\ jY\sin\beta l & \cos\beta l \end{bmatrix} \tag{3.7}$$

where Z_{adl} is the impedance of the ADL layer, Z and Y the characteristic impedance and admittance of the transmission lines with propagation constant β. The complete stratification can be represented as a cascade of such ABCD matrices. The ABCD matrix of the entire structure can be used to retrieve the equivalent permittivity of the medium, as in [24]. Alternatively, the ABCD matrix can be transformed into a S-parameter matrix, from which the permittivity is retrieved using the technique described in [25, 26].

The extracted effective permittivity from a homogenized ADL slab is maximum for normal incidence and decreases with oblique incidence angles as shown in Fig. 3.7. The dependence of the extracted epsilon with the angle of incidence of the plane wave indicates that the equivalent medium is anisotropic.

In the TM case, the extracted epsilon attains the permittivity of the host medium for grazing incidence as it can be observed in Fig. 3.7. This is because the patches become orthogonal to the electric field of the plane wave for high incidence angles. Whereas, for TE incidence the electric field still feels the presence of the patches for grazing incidence, as the field is parallel to the patches. Hence, the retrieved permittivity does not tend to the epsilon value of the host substrate.

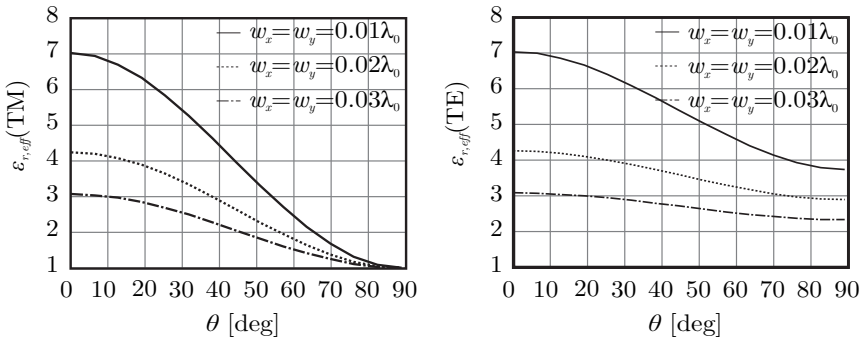

Figure 3.7: Variation of effective dielectric constant of the ADL slab with angle of incidence of (a) TM and (b) TE polarized plane wave.

3.4 Surface wave characteristics of ADL

A study of the dispersion characteristics of finite ADL slabs was described in [23], based on the ADL spectral Green's functions. The surface wave and leaky wave modes supported by the slab are associated with polar singularities of the spectral Green's functions. The most important findings, that will be useful during the design phase, are the following:

- An ADL stack hosted by free space does not support TM surface waves but only leaky waves.
- An ADL stack hosted by free space can support the propagation of TE leaky waves, as well as TE surface waves when its height is greater than $0.3\lambda_{eff}$ (λ_{eff} is the effective wavelength of the medium for normal incidence).
- An ADL stack hosted by a dielectric substrate does not introduce additional TM surface waves, but only the ones the would be supported by the host substrate itself, in absence of the ADL.

The presence of TE surface waves supported by the ADL slabs must be taken into account when designing the array. In fact, the propagation of these modes can lead to scan blindness for wide scan angles, limiting the bandwidth.

Chapter 4

Analytical Tool and Array Design

4.1 Introduction

In this chapter, an analytical tool is presented to design a wide-band connected array of slots loaded with artificial dielectric layers (ADLs). The formulation exploits the analytical spectral Green's functions of the connected arrays and ADL, as discussed in the previous chapters. The analytical tool takes into account all the higher-order-mode interactions between array and ADL, even when the array is located at a distance in order of one hundredth of the wavelength from the ADL. Using this tool, a single polarized array with -10 dB matching over an octave bandwidth and scanning up to $50°$ is designed. The design is extended to a dual-pol configuration by the introduction of an orthogonal slot and performance similar to that of single-pol array is achieved.

4.2 Analytical tool

The impedance of the connected array loaded with ADL, is formulated using the spectral Green's function of the connected array of slots and the ADL. The input impedance of the connected array of slots was given in Chapter 2, in equations (2.1) and (2.2).

The expression of the input impedance was given in terms of the xx-

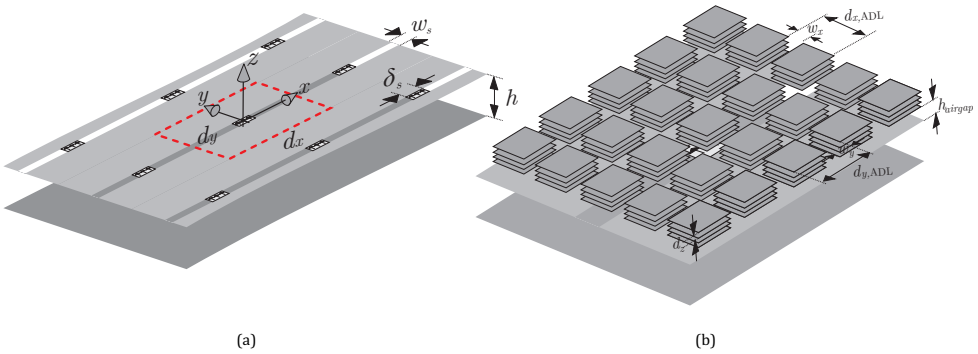

Figure 4.1: (a) Connected array of slots in free space in the presence of a backing reflector and (b) a unit cell of the array loaded with ADL.

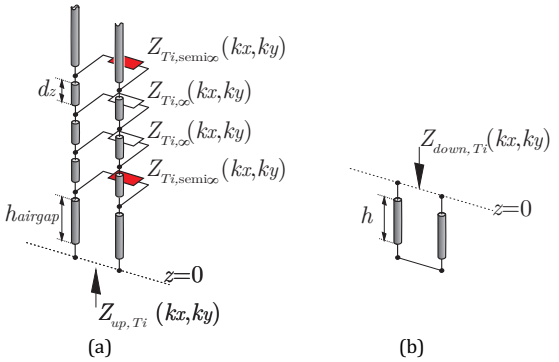

Figure 4.2: An equivalent transmission representation of a finite height ADL for a generic TE and TM plane wave.

component of the spectral Green's function for stratified media (see Eq. (2.3)). The Green's function depends on the current solutions of two transmission line models (for TE and TM), representing the arbitrary stratification. These currents are induced due to a unitary voltage source located at $z = 0$ and they can be expressed as $1/Z_{\mathrm{Ti}}$, where Ti can refers to either TE or TM. For the case of connected array loaded with ADL, Z_{Ti} is the parallel combination of the impedances $Z_{up,\mathrm{Ti}}$ and $Z_{down,\mathrm{Ti}}$, which represent the upper and lower stratification, as depicted in Fig. 4.2. The ADLs are assumed to be infinite along the x- and y-axes, whereas the finiteness along the transverse axis (z) is taken into account by using the semi-infinite approximations for the edge layers. The impedance $Z_{up,\mathrm{Ti}}$ can be found by solving

the transmission line circuit as shown in Fig. 4.2(a). It should be noted that the values of this impedance are function of k_x and k_y, which represent the characteristic propagation constant of the incidence plane wave. Similarly, the impedance $Z_{down,\mathrm{Ti}}$ is calculated by transforming a short circuit due to the backing reflector that is located at a height h from the array plane along negative z-axis.

Consequently, the TE and TM impedance of each layer can be expressed as follows:

$$Z_{\infty,\mathrm{TM}} = \frac{-j}{B_{s\infty}}, Z_{\mathrm{semi}\infty,\mathrm{TM}} = \frac{-j}{B_{s,\mathrm{semi}\infty}}$$
$$Z_{\infty,\mathrm{TE}} = \frac{-j}{B_{s\infty}\left(1-\frac{k_\rho^2}{k_0^2}\right)}, Z_{\mathrm{semi}\infty,\mathrm{TE}} = \frac{-j}{B_{s,\mathrm{semi}\infty}\left(1-\frac{k_\rho^2}{k_0^2}\right)}. \tag{4.1}$$

where k_ρ is $\sqrt{k_{xm}^2 + k_{xm}^2}$ and k_0, the propagation constant of free space. The susceptance of each ADL layer was given in (3.4) and (3.5). Note that the expression in (4.1) is more general than the ones in (3.1 and 3.2), since it is valid also for wavenumber outside the visible spectrum, associated with inhomogeneous plane waves.

4.2.1 Numerical example - single ADL slab

In this section, a numerical example is presented, with the geometry as shown in Fig. 4.1, that makes use of a MATLAB code to solve the transmission line based equivalent circuit outlined in Fig. 4.2. These results are verified using a commercial EM solver [32]. The dimensions of the connected array are summarized in Tab. 4.1, whereas those of the ADL are listed in Tab. 4.2.

$d_x = d_y$	w_s	δ_s	h	h_{airgap}
$0.47\lambda_0$	$\lambda_0/48$	$\lambda_0/12$	$\lambda_0/12.5$	$\lambda_0/80$

Table 4.1: Dimensions of the connected array in terms of free space wavelength at the maximum frequency.

For normal incidence, an effective dielectric constant of 8.4 is obtained for the ADL dimensions in Tab. 4.2. A total of 5 layers are used in the ADL

$d_{x,ADL} = d_{y,ADL}$	$w_x = w_y$	d_z
$0.16\lambda_0$	$0.009\lambda_0$	$0.0063\lambda_0$

Table 4.2: Dimensions of the ADL in terms of free space wavelength at the maximum frequency.

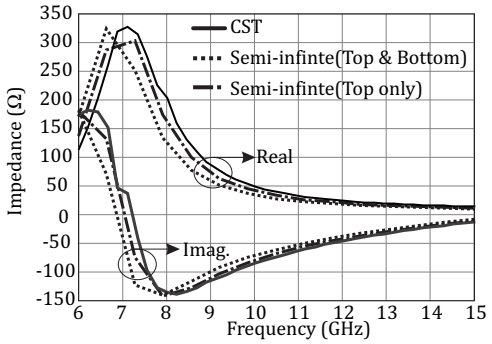

Figure 4.3: Input impedance of the connected array of slots loaded with ADL for normal incidence, for geometrical parameters given by Tables 4.1 and 4.2.

design, refer Fig. 4.1. The first layer is placed at a very small distance from the array plane ($\lambda_0/80$). Figure 4.3 reports the results for the active input impedance of the array using the analytical tool, compared with the full-wave simulations. Two cases are considered: in the first, both the first and last layers of the ADL stack are approximated with a semi-infinite solution for the layer impedance; in the second case, only the top layer is modeled using the semi-infinite solution. It can be observed that the second case leads to a slightly better comparison with the full-wave simulations. That is because the first ADL layer is located in the close proximity of the ground plane on which the slots are etched, coupling reactively with it. For larger distances from the ground plane, a semi-infinite approximation can be used also for the first layer. A very good comparison is also obtained for scanning toward 50° in the E- and H-planes, as shown in Fig. 4.4.

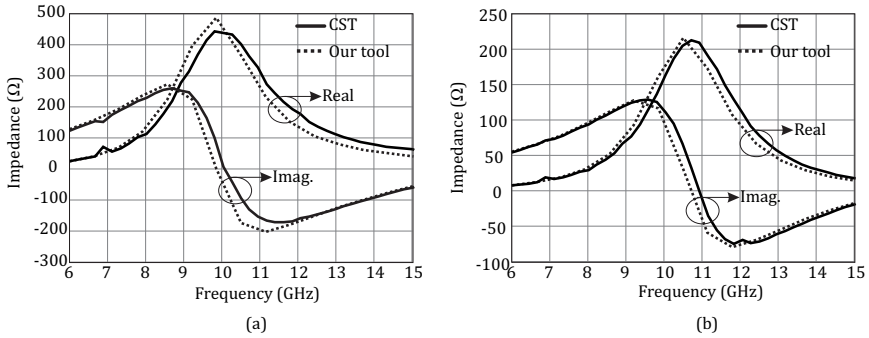

Figure 4.4: The input impedance of the connected array of slots loaded with ADL for scanning at 50° in (a) H- plane (b) E- plane.

4.3 Design of a wideband and widescan ADL enhanced connected array

In this section, an array design is presented that has -10 dB matching over a bandwidth exceeding one octave, in the frequency range from 7 to 14.5 GHz, and scanning capabilities up to 50° in all azimuthal planes.

It is well-known in the literature [28] that a broadband impedance transformation can be achieved using multi-section transformers. This concept can be used to design a multi-section slab to match the impedance of the array, which is in the order of 50 Ohms to connect to a coaxial feed, to the one of free space. Depending on the type of transformation (for e.g Chebyshev, binomial), multiple dielectric slabs with different permittivity are used. Each matching layer should have a thickness in the order of a quarter wavelength at the central frequency within the band of operation. However, due to the electrical thickness of the slab, surface waves are excited when scanning, which results in scan blindness.

In [10], it was shown that high permittivity slabs of quarter wavelength effective height can be realized using ADLs. These slab do not support surface waves as they are realized on a host substrate which is electrically thin. Moreover, the antenna which is placed below the ADL has a high front-to-back ratio due to the high dielectric contrast between the upper and the lower half spaces. In the subsequent section, a multi-section ADL design is presented. By exploiting the analytical Green's function tool presented

Parameter	Slab1	Slab2	Slab3
$d_{x,ADL} = d_{y,ADL}$	$0.093\lambda_0$	$0.093\lambda_0$	$0.093\lambda_0$
w_x	$0.009\lambda_0$	$0.0068\lambda_0$	$0.01\lambda_0$
d_z	$\lambda_0/157$	$\lambda_0/60$	$\lambda_0/10$
# layers	5	6	3
ε_{eff}	16.5	7.03	2.17
ε_{host}	2.2	1	1

Table 4.3: Dimensions of the three ADL slabs

in the previous section, the array can be easily optimized to achieve the required performance.

4.3.1 ADL transformer design

A broadband matching from 7 to 14.5 GHz can be realized using three dielectric slabs having permittivity 2.1, 7 and 16.5 respectively. These three different dielectric constants can be realized by varying the geometrical parameters of the ADL ($d_{x,ADL}$, $d_{y,ADL}$, w_x, w_y and d_z in Fig. 4.1(b)). In this specific design, the periodicity along the lateral axes ($d_{x,ADL}$, $d_{y,ADL}$) is set to $0.093\lambda_0 = 1.862$mm, λ_0 being the wavelength in free space at 15 GHz. These dimensions ensure that the patches are smaller then a quarter wavelength over the entire frequency range of operation. Such a small size yields very low ohmic losses, in virtue of the non-resonant nature of the metal patches. Moreover, under the hypothesis of small periods, the analytical tool developed in [22, 23] remains valid with high accuracy.

The dimensions used in the design of the ADL transformers are reported in the table 4.3, where the values are given in terms of λ_0, which is the wavelength at 15GHz.

The extracted effective dielectric constant for each of the slab for TM and TE incidence is shown in Fig. 4.5(a) and (b), respectively, for infinite cascade configuration.

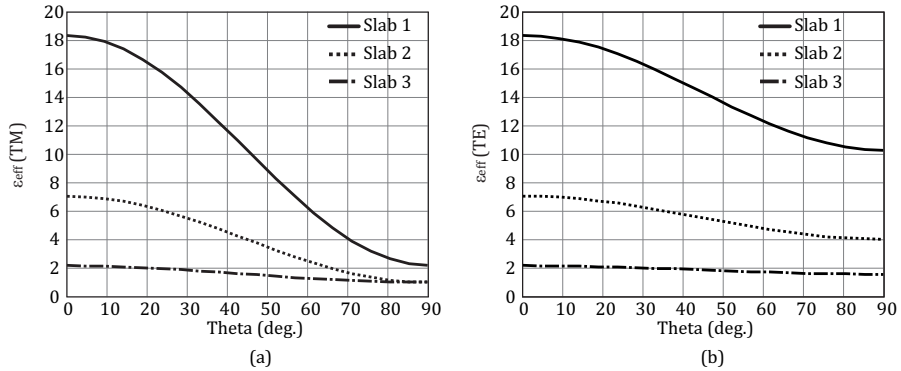

Figure 4.5: Variation of the extracted epsilon with angle of incidence for the ADL slabs for (a) TM and (b) TE incidence.

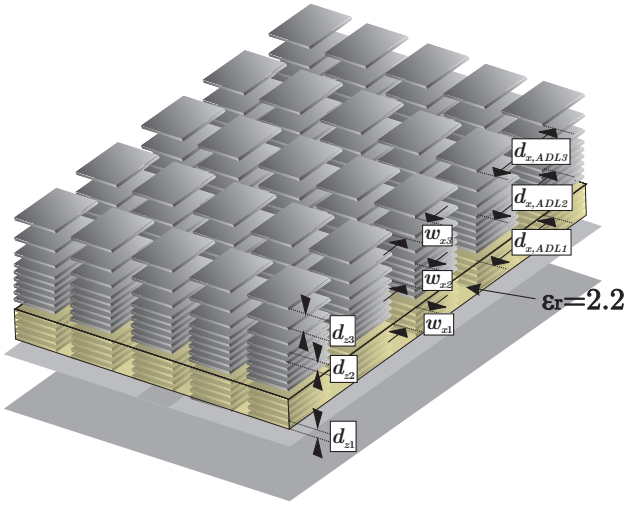

Figure 4.6: Complete array stack.

4.3.2 Single-pol design

The dimensions of the connected array used in the single-pol design are the same as in Tab. 4.1. The parameters w_s and δ_s are used to fine tune the array input impedance to be matched to 55Ω across the required bandwidth. The three ADL slabs presented in the previous section are stacked on top of the array plane at the distance h_{airgap}. The unit cell configuration of the array loaded with the ADL slab is shown in Fig. 4.6(a). The equivalent spectral transmission line representation is depicted in Fig. 4.6(b).

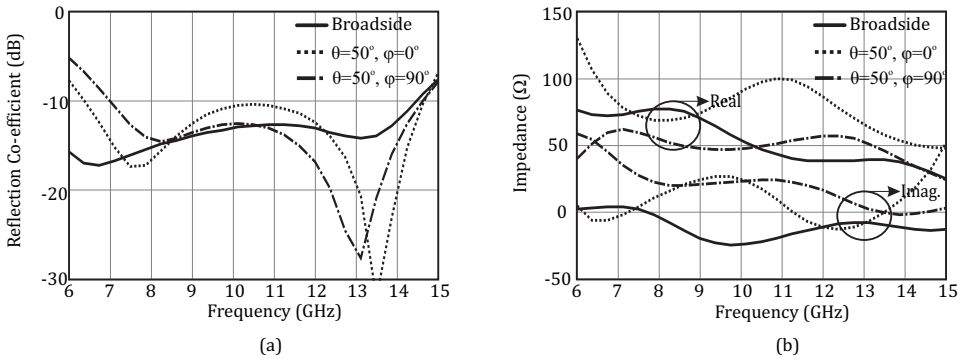

Figure 4.7: (a) Active reflection co-efficient and (b) active input impedance of the array.

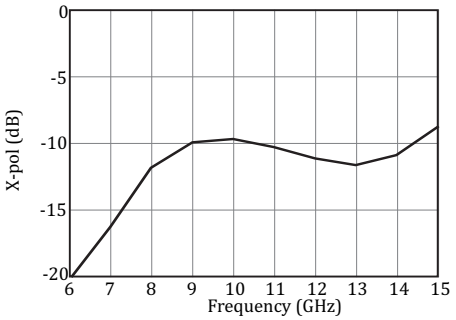

Figure 4.8: Cross-pol performance in the diagonal plane of a single polarized connected array of slots loaded with ADL.

The reflection coefficient of the array when matched to 55Ω is shown in Fig.4.7(a), for broadside and scanning to 50° in E- and in the H-plane. The active input impedance of the array is shown in Fig. 4.7(b). These results have also been validated with CST [32] and not shown here for the sake of brevity. The −10 dB matching of the array is from 7 to 14.5 GHz. The prominent feature of this design is that the backing reflector is placed at a distance of $0.08\lambda_0$ form the array plane. This is possible due to high front-to-back radiation ratio that has been achieved using ADL in a multi-slab configuration.

The cross polarization of this array is less than −20 dB in the main planes. Whereas, for scanning in the diagonal plane at $\theta = 50°$, it has values of about −10 dB in the operative frequency band, as shown in Fig.4.8.

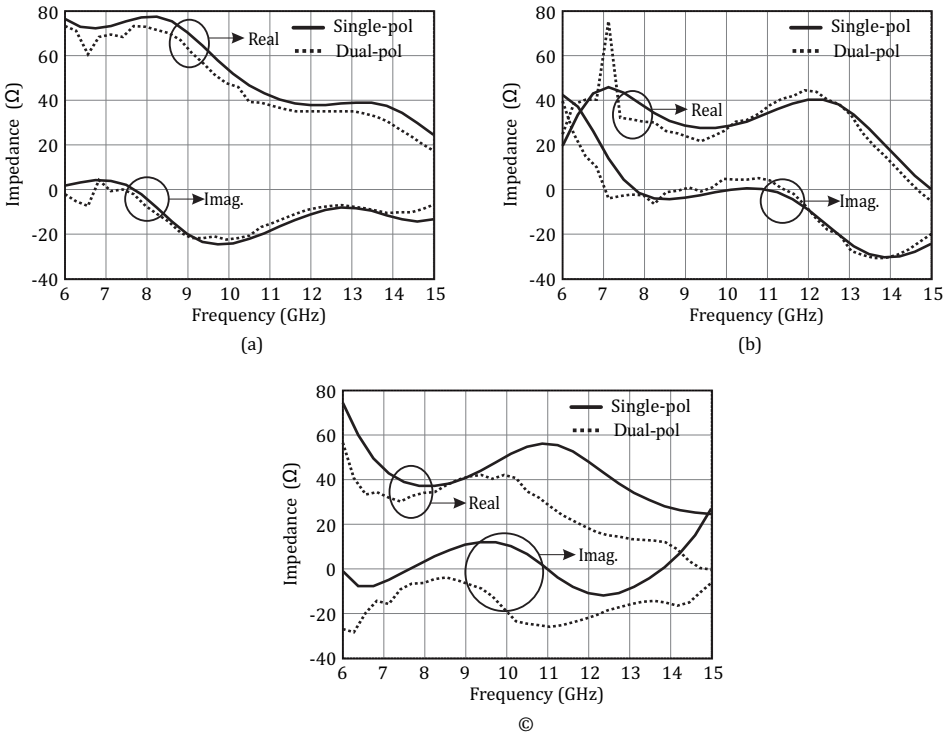

Figure 4.9: Impedance comparison between the single-pol and dual-pol array for scanning in (a) broadside, (b) 50° in E-plane and (c) 50° in H-plane.

It is 5 dB more than the expected level of −15 dB, which is the typical behaviour of any linearly polarized electric/magnetic dipole. This is because of the addition of a high permittivity slabs is associated with higher cross-polarization levels, as it was demonstrated in [27]. A similar behavior can be observed for ADL slab, which, in terms of cross-polarization levels, behaves similar to a homogeneous slab with the same permittivity of the ADL for normal incidence.

4.3.3 Dual-pol design

The design of a single-pol array is extended to the dual-pol configuration by considering an array of slots orthogonal to the one shown in Fig. 4.1(a), i.e. along y axis. As the analytical tool deals only with the design a single-pol array, one has to resort to a commercial simulator to model the dual-pol array. In Fig. 4.9, the active input impedance is shown for the cases of single-

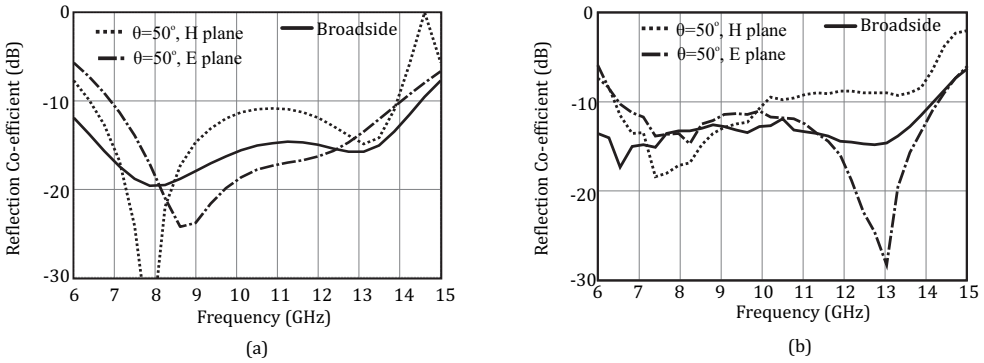

Figure 4.10: Active reflection co-efficient of (a) single-pol array and (b) dual-pol array.

and dual-polarized arrays, for broadside and scan on the main planes. It is apparent that the impedance does not change for broadside and scan in the E-plane, while different values are obtained for the case of scanning in the H-plane. In this latter case, the real part of the impedance of the dual-pol design becomes lower at the higher frequencies and almost zero at 15 GHz, while the imaginary part is highly capacitive.

As a consequence, the simulated matching performance of the dual-pol design, shown in Fig. 4.10(b), differs from the one of the single-pol array shown in Fig. 4.10(a). It can be seen that -10 dB matching of the array for normal incidence as well as 50° scanning in the E-plane is the same as that of the single-pol design. However, for 50° scanning in the H-plane the reflection coefficient degrades.

Crossing slot resonance

In order to investigate the reason for the performance degradation when the array is scanning in the H-plane, the electric field distribution on the slots is analyzed.

The case in which only one polarization is excited (active slots), with the crossing slot being passive, is considered. When the array is scanning in the E-plane, there is no progressive phase shift between the successive feeds in the active slots. As a consequence, the electric fields generated by two feeds in adjacent unit cells have the same amplitude and phase and give

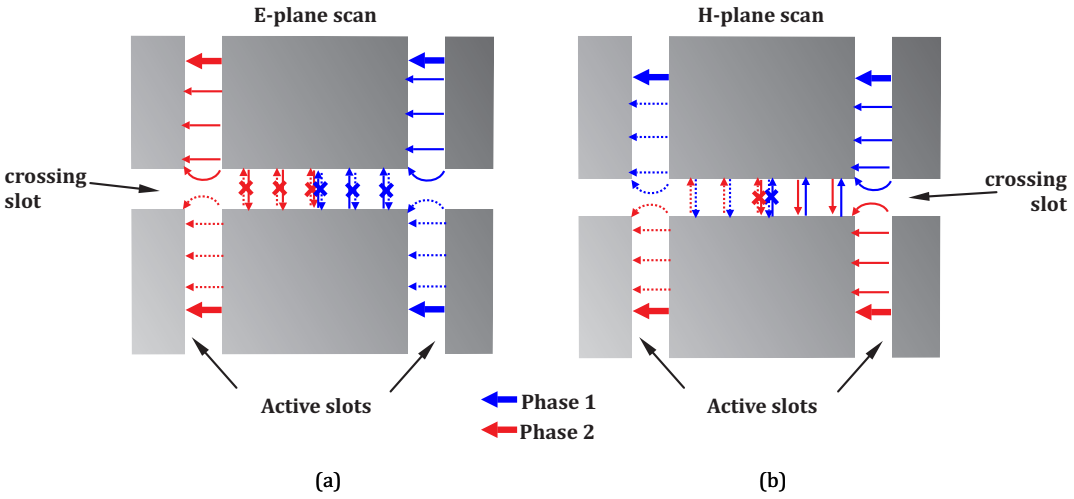

Figure 4.11: Representation of the vector electric field lines in the slots when the array is scanning in (a) E-plane and (b) H-plane.

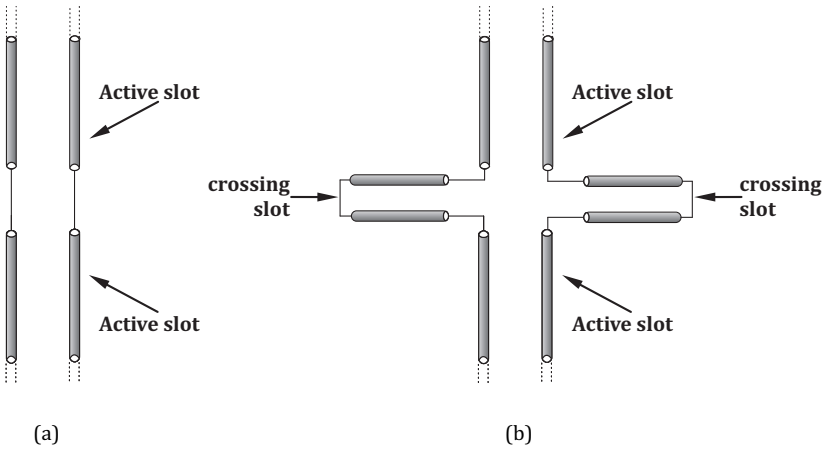

Figure 4.12: Equivalent transmission line representation of the slots scanning in (a) E-plane and (b) H-plane.

equal and opposite contributions in the crossing slots. This yields a perfect cancellation of the electric field across the entire orthogonal slot, as depicted in Fig. 4.11(a).

Differently, when array is scanning in the H-plane, there is a progressive phase shift between two successive feeds in the active slots. Due to this phase difference, the electric fields from these feeds do not have the same phase,

hence they do not cancel out in the crossing slot. A perfect cancellation is only occurring in the center of the orthogonal slot, due to the electric field generated by the feeds in the parallel, as shown in Fig. 4.11(b).

The equivalent transmission line representation of the slots scanning in the E- and H-planes is shown in Fig. 4.12(a) and (b), respectively. For E-plane scanning, since the electric field vanishes across the entire orthogonal slots, the active slots behave as they were isolated (single-pol case). Thus, the equivalent transmission line representation of the slots is characterized by short circuits at the junction (as shown in Fig. 4.12(a)). When scanning in the H-plane, the electric field vanishes only at the center of the crossing slot, which can thus be represented by a short stub (Fig. 4.12(b)). When the electric length of the stub becomes a quarter wavelength, a resonance is observed in the active input impedance of the active slots. This is evident from the Fig. 4.9(c), where the real part of the input impedance becomes zero at about 15GHz, which corresponds to a quarter-wave long stub.

Cross polarization

In order to investigate the effect of the ADL on the cross-pol performance of the array, three geometries have been simulated, as depicted in Fig. 4.13: the first geometry consists of a dual-pol array of slots load with a dielectric slab with relative permittivity of 2.2 (Fig. 4.13(a)); the second geometry is the same array where the slab has been loaded with ADLs, achieving an equivalent permittivity of 16.5, for normal incidence(Fig. 4.13(b)); the final geometry is the complete structure with two addition ADL slabs, hosted in free space (foam in a realistic design). The cross-pol performance associated with the three structures is reported in Fig. 4.14), for scanning to $\theta = 50^\circ$ in the diagonal plane. The cross-pol levels are the lowest in the case without ADL and deteriorates with the addition of the ADL slabs. The levels associated with the three geometries is still below -10 dB.

The cross-pol level of the dual-pol array is represented by the black solid curve as shown in Figure 4.14. It still varies around 10 dB, similar to the case of single-pol array.

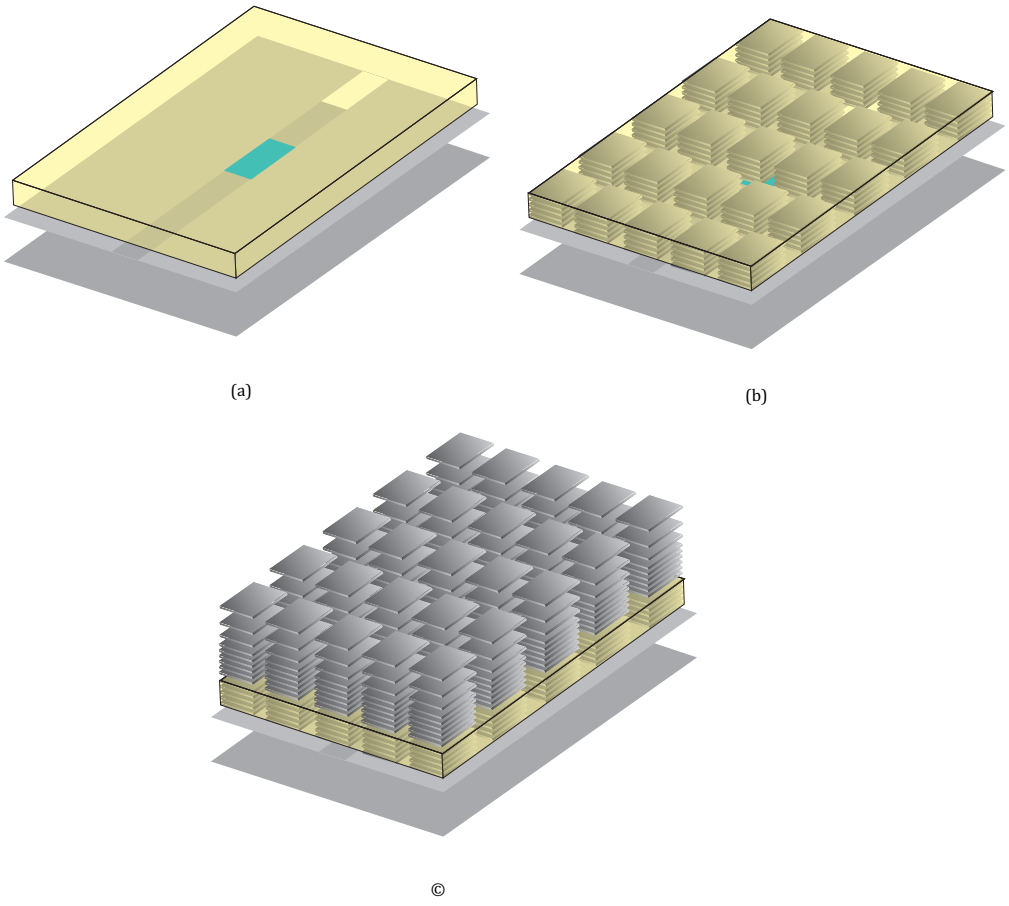

Figure 4.13: (a) Connected array with no ADL, (b) array loaded with single ADL slab and (c) array loaded with the entire ADL stack.

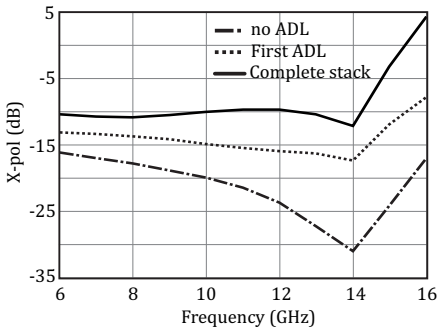

Figure 4.14: Cross-pol performance for different configurations.

Chapter 5

Prototype Design

5.1 Introduction

This chapter deals with the design of a realistic array, with the aim of fabricating a prototype demonstrator. The design is based on the ideal structure presented in the previous chapter, but is fine tuned and re-optimized to include fabrication details and achieve similar performance as the ideal case. The main features addressed in this chapter are two: the inclusion of adhesive layers to bond the printed circuit boards (PCBs) composing the ADL stack, both in the analytical tool and in the CST simulations; the design of a realistic feed structure for the array elements, including a transition from the microstrips, used to feed the slots, to the coaxial connectors.

5.2 Prototype design details

A realistic fabrication of the multi-layer structure resenting the array loaded by ADL is reported in Fig. 5.1. The ADL slabs that were hosted in free space for the ideal design case, can be realized by using slabs of Rohacell Foam ($\epsilon = 1.06$). More specifically, the metal patches can be printed on a thin dielectric film, LG4002 ($\epsilon = 2.32$ and thickness, h=0.05mm) and this layer is then glued on the the foam using adhesive film CuClad 6250 from Arlon ($\epsilon = 2.32$ and h=0.038mm), as shown in Fig. 5.2. The first ADL slab is instead realized with Rogers RO5880 ($\epsilon = 2.2$), where the ADL can be printed on either sides of the substrate, refer Fig. 5.3.

The active reflection co-efficient of the array with the inclusion of the

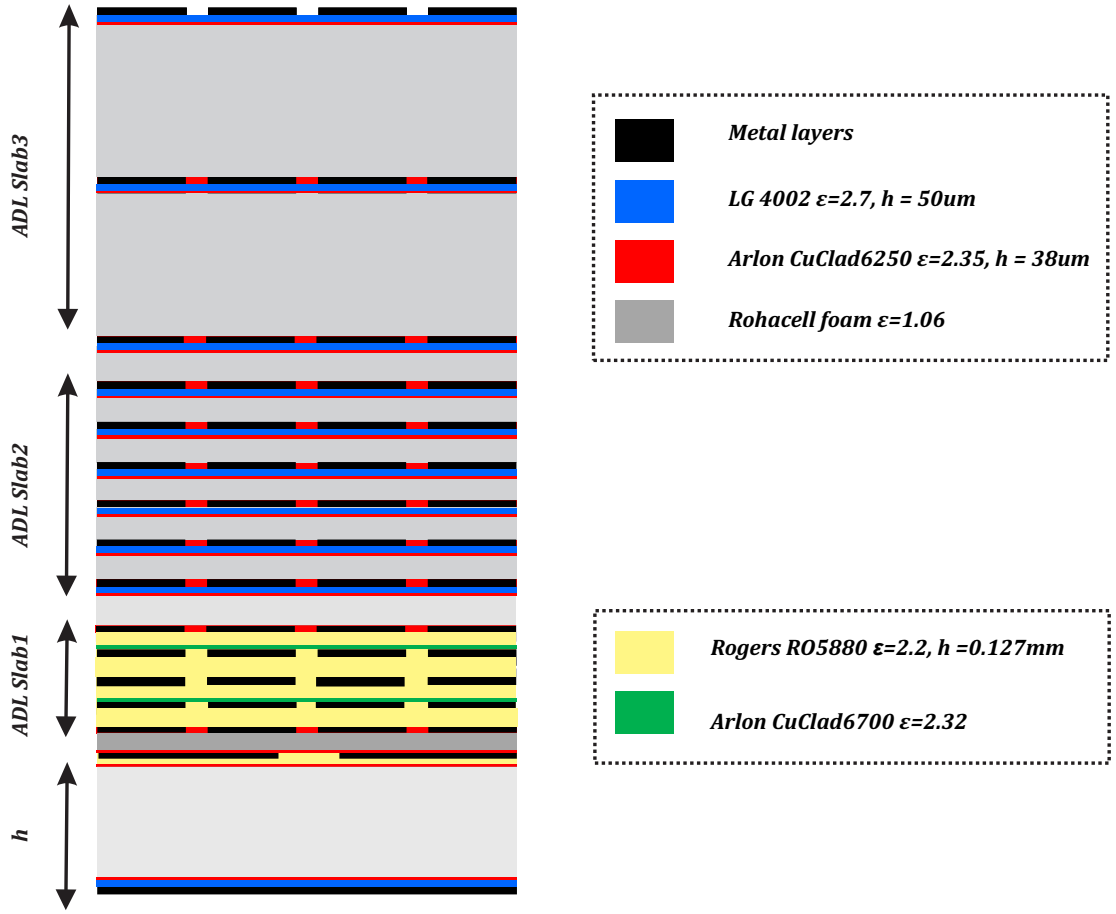

Figure 5.1: Complete array with the inclusion of bonds.

bonds is shown in Fig. 5.4(b). From the Fig. 5.4(a) and (b), it is clear that the inclusion of the bondings has a significant impact on the performance of the array, as it leads to a strong degradation of the reflection coefficient across the entire frequency band. This is due to the fact that the numerous adhesive films required have a total thickness that is not negligible with respect to the total height of the structure. Consequently, the connected array and the ADL must be redesigned with the inclusion of the adhesive layers.

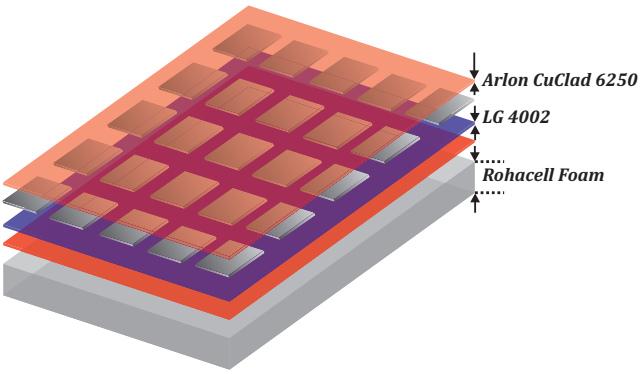

Figure 5.2: Exploded view of ADL printed on foam with the inclusion of bond.

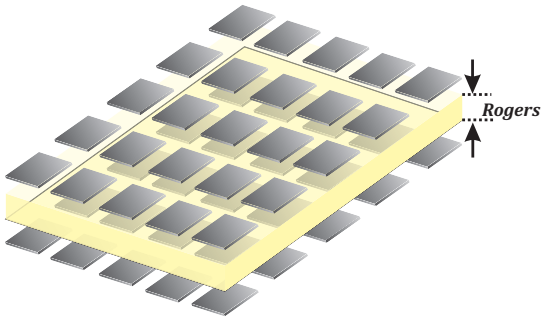

Figure 5.3: Exploded view of ADL printed on rogers substrate.

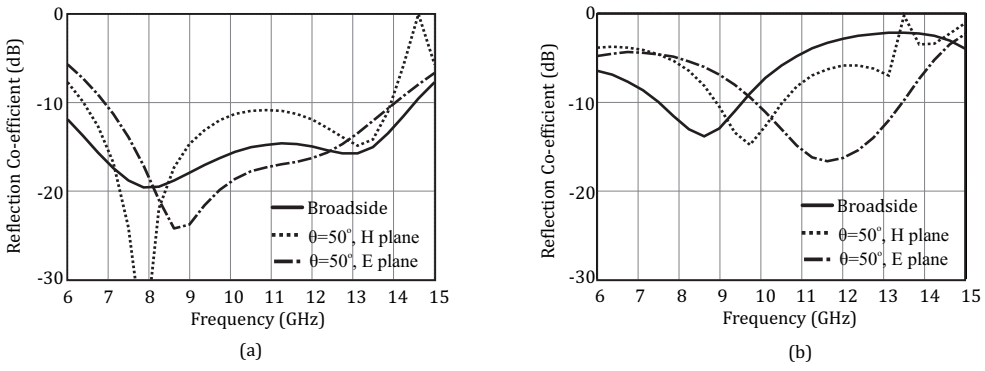

Figure 5.4: Active reflection co-efficient of the single-pol array (a) without bonds and (a) with bonds.

Parameter	Slab1	Slab2	Slab3
$d_{x,ADL}$	1.832mm	1.832mm	1.832mm
w_x	0.14mm	0.3mm	0.4mm
d_z	0.127mm	0.476mm	3.07mm
# layers	2	3	2
ε_{host}	2.2	1	1

Table 5.1: ADL dimensions after the inclusion of adhesive films in the array.

Parameter	Dimension
d_x	9.31mm
d_y	9.31mm
w_s	0.22mm
δ_s	2mm
h_{airgap}	0.635mm
h	1.6mm

Table 5.2: Array Dimensions after the inclusion of adhesive films.

5.2.1 Array performance

Single-pol array

After re-optimization of the parameters to obtain similar performance to the case without bondings, the final ADL and array dimensions are the ones listed in Table 5.1 and 5.2, the complete stack is depicted in Fig. 5.5 .

The active reflection coefficient and the input impedance of this array are shown in Fig. 5.6(a) and (b), respectively, for broadside and 50° scanning in the H- and E-plane. The single polarized array is matched from 7 to 14 GHz with the inclusion of the bonds.

Dual-pol array

Figures 5.7(a) and (b) show the performance obtained by simply extending the single-pol design to a dual-pol one, by including an orthogonal set of identical slots with the same geometrical parameter and keeping the ADL dimensions unvaried. The -10 dB matching of the dual-pol array is from

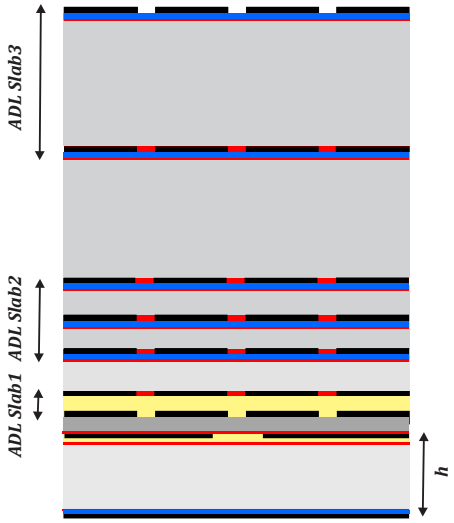

Figure 5.5: ADL stack after re-optimization.

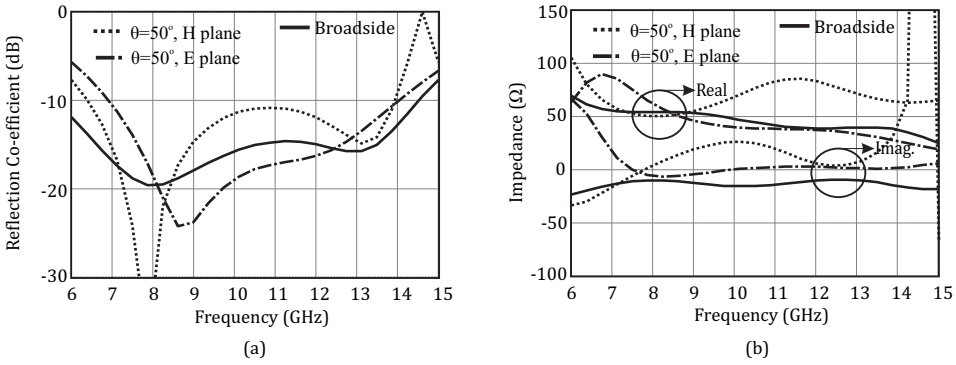

Figure 5.6: (a) Active reflection coefficient and (b) active input impedance for broadside and 50° scanning of the single-pol array with adhesive films.

7.5 to 10.5 GHz, which is smaller in comparison to the single-pol design. The deterioration in the performance is due to the crossing slot resonance, discussed in the previous chapter. Bandwidth of this array can be improved by adding an inductor in series with the array feed.

The value of the inductance to be added is found analytically by making use of the impedance values obtained from the CST simulations and performing a parametric study as shown in Fig. 5.8. When an inductance of 0.22 nH is added in series with the array feed, a -10 dB matching from 7.5

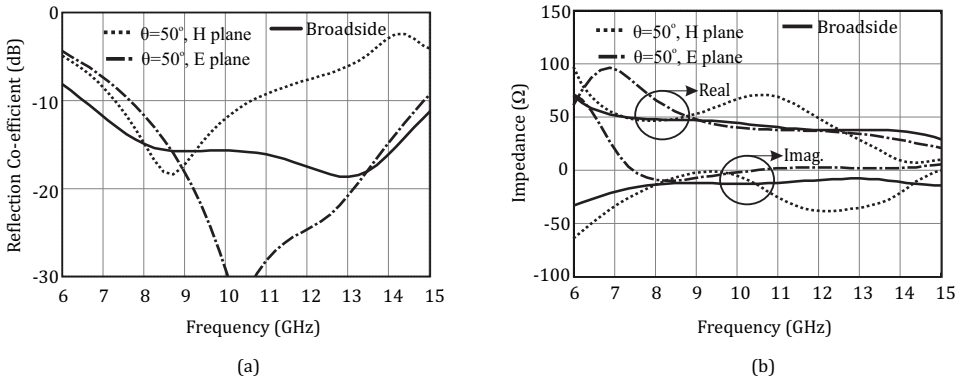

Figure 5.7: (a) Active reflection co-efficient and (b) active input impedance of the dual-pol array with adhesive films, for broadside and 50° scanning in the main planes.

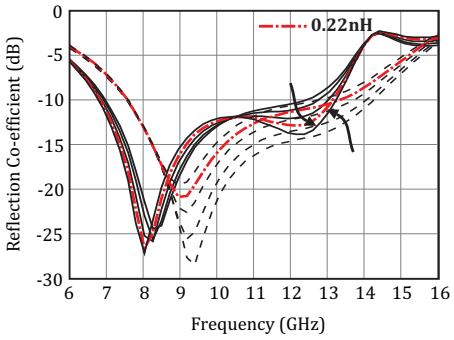

Figure 5.8: The active reflection co-efficient variation with the added inductance values from 0.1 to 0.22 nH. Optimal bandwidth from 7.5 to 13 GHz is achieved for an inductance value of 0.22 nH.

to 13 GHz is achieved as shown in the Fig. 5.9. With further increase in the inductance value, the bandwidth reduces in the orthogonal plane due to high imaginary part of the impedance. Hence 0.22nH is an optimal value. The achievable bandwidth with 0.22nH inductance is shown in Fig. 5.9.

In reality the slots are fed using microstrip coupling, which are realized on a rogers substrate, of thickness 0.127 mm, below the array plane. Hence, one has to optimize the width of the microstrip to ensure that the real part of the input impedance for scanning in the H-plane is close to the values obtained at the array plane. This is critical as the bandwidth of the array is

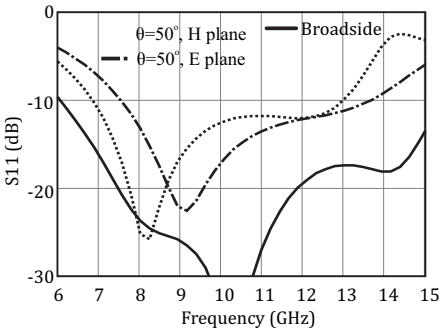

Figure 5.9: Active reflection coefficient of the dual-pol array after adding an inductance of 0.22 nH.

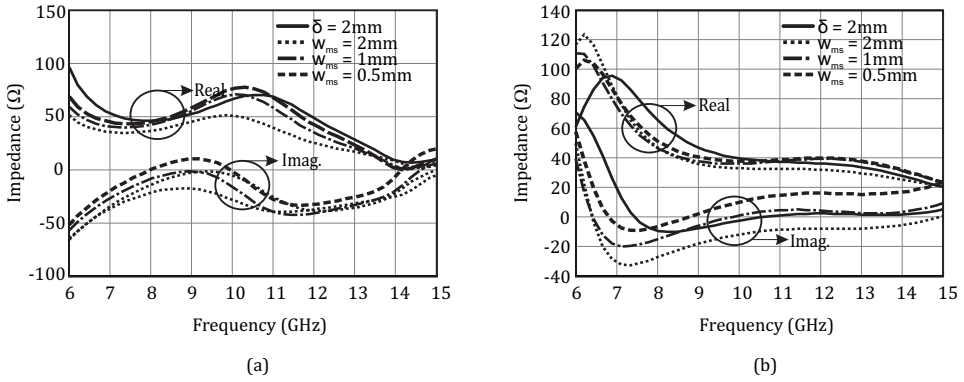

Figure 5.10: Active impedances of the array scanning at 50° in (a) H- plane and (b) E- plane for different widths of the microstrip used below the slots.

limited by the low real impedance value at the higher frequency band.

From Fig. 5.10(a) it is observed that the width of the microstrip is reduced 0.5mm to obtain the real part of the input impedance close to the values that are evaluated on the array plane. With the reduction in the width the imaginary part of the impedances becomes very inductive which is evident in the Fig. 5.10. Hence the inductance to be added in series with the microstrip should be reduced to ensure that there is no over compensation.

Hence an inductance of 0.09nH is added in series with the microstrip line below the slots to obtain an active reflection co-efficient similar to the one with no bonds. This inductance is realized by narrowing of the microstrip line as shown in Fig. 5.11.

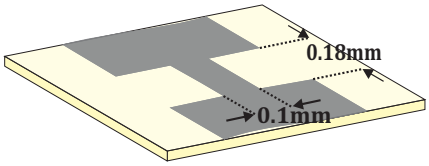

Figure 5.11: Inductance realized by narrowing the microstrip transmission line.

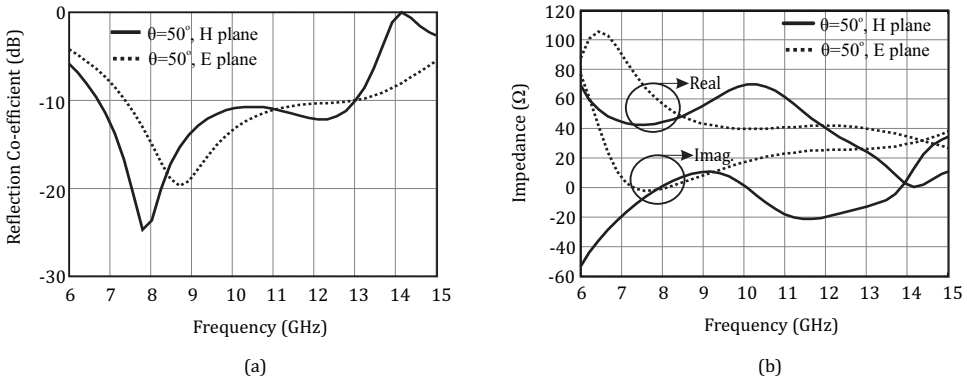

Figure 5.12: (a) Active reflection co-efficient and (b) active input impedance of the dual-pol array with an inductor in series with the microstrip feed scanning at 50° in both the E- and H-planes.

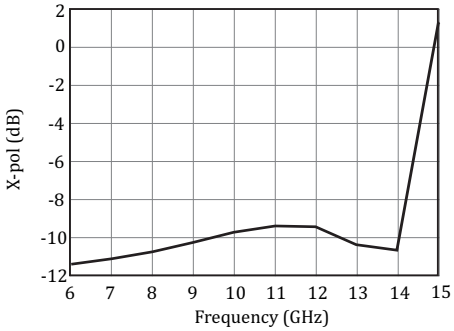

Figure 5.13: Cross polarization performance of the dual-pol array with adhesive films along the diagonal plane.

The final active reflection co-efficient and cross-pol performance of the dual-pol array after incorporating the optimized microstrip width below the

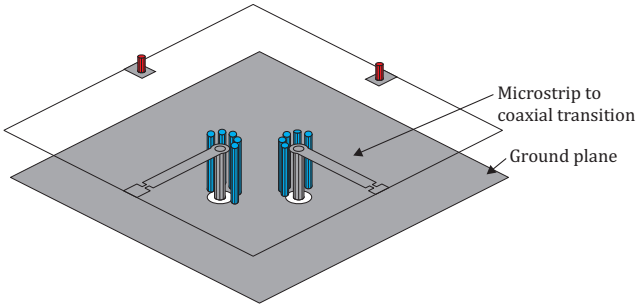

Figure 5.14: Microstrip to coaxial transition to realize a quarter wavelength transformer.

Dimensions	
diameter of central conductor	0.28mm
diameter of outer conductor	0.2mm
length of coaxial	1.6mm
width of microstrip	0.4mm
length of microstrip	2.7mm

Table 5.3: Microstrip and coaxial physical dimensions.

slots and an inductance of 0.09nH in series with it is shown in Fig. 5.12 and Fig. 5.13. The array is matched to an impedance of 39Ω. The broadside active reflection co-efficient and the active impedance are not shown in the figure.

5.2.2 Feed network design

Besides designing the array, the feed network has to be implemented to match the array to a 50Ω SMP connector. Since the array is matched to 39Ω, it is required to transform this impedance to 50Ω at the ground plane using a quarter wavelength transformer. This transformer is realized using a microstrip to integrated coaxial transition as shown in Fig. 5.14.

The dimensions of the microstrip and the coaxial line is listed in Table 5.3. The performance of the quarter wavelength transformer in terms of its reflection co-efficient is shown in Fig. 5.15, where port1 is placed at the end of the microstrip and port2 at the end of the coaxial line.

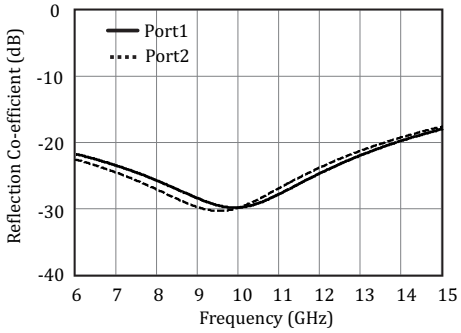

Figure 5.15: Reflection co-efficient of the quarter wavelength transformer.

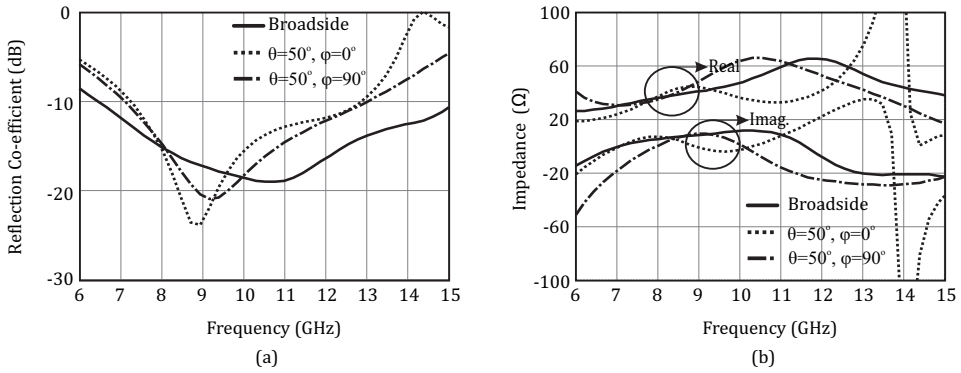

Figure 5.16: (a) Active reflection co-efficient and (b) active impedance of the dual-pol array for broadside and 50° scanning in E- and H-planes with the inclusion of the quarter wavelength transformer.

Performance of the dual-pol array with the feed network

The performance of the dual-pol array with the feeding network in terms of the active reflection co-efficient and cross polarization level is depicted in Fig. 5.16 and 5.17. The -10 dB matching is from 7 to 13 GHz, while the cross-pol level is lower than -11 dB across the entire bandwidth. It should be noted that a grid will be included below the array plane to provide stability in the fabrication design along with a coaxial to microstrip transition behind the backing reflector.

The feed network with the inclusion of the grid will be as shown in Fig. 5.18. There will not be a difference in the cross-pol performance of the array with the inclusion of the grid, however there might be reduction in the -10

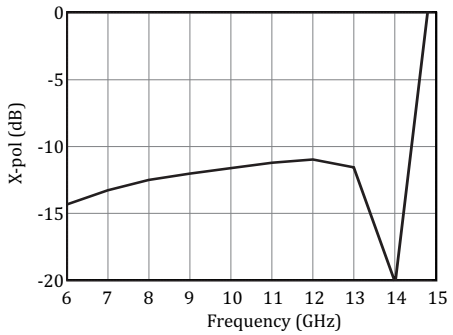

Figure 5.17: Cross-pol performance of the dual-pol array with adhesive layers and transformer.

dB matching.

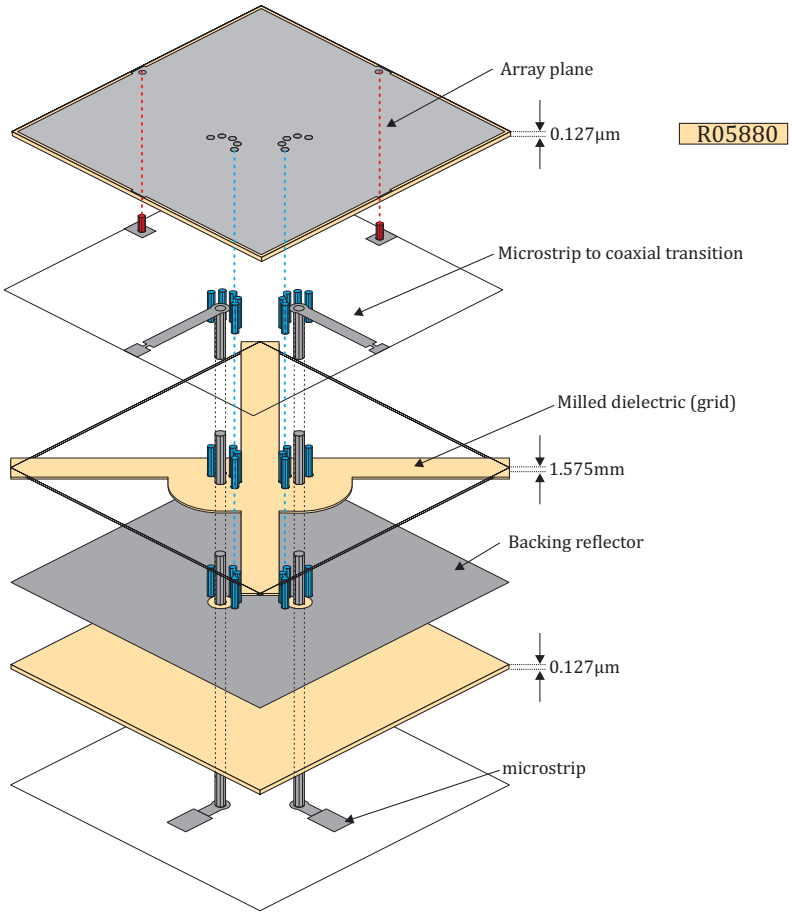

Figure 5.18: A realistic feed network of the array.

Chapter 6

Conclusions and Future Developments

In this thesis, the design of a connected array of slots loaded with ADLs has been presented. The proposed structure achieves wideband and wide-scan capabilities and has several advantages with respect to the existing solutions. The salient features of the design are the following:

- Dual-polarized wideband wide-scan arrays, based on connected array of dipoles or tapered slot antennas, are implemented resorting to vertical arrangements of printed circuit boards (PCBs). On the contrary, the structure presented in this thesis is completely planar and realized with a single multi-layer PCB, with consequent reduction of the cost and the complexity of the array.

- ADLs are used in place of real dielectric superstrates, as they are characterized by much better efficiency in terms of surface-wave loss. This characteristic property is due to the anisotropic nature of the ADL.

- The presence of the ADL allows using slot elements in the array without exciting parallel plate waveguide mode between the array plane and the backing reflector. The selection of slot elements leads to a much easier implementation of the feed with respect to connected dipole arrays. The slots are fed by means of an aperture-coupled microstrip line. This is not the case for dipole elements, for which balanced-to-unbalanced

(balun) transitions are required, which often constitute the limiting factor for the achievable bandwidth.

- For the design of the array loaded with ADL, including the adhesive layers, an analytical tool can be used which allows to estimate the performance of the array with very small computational resources. More specifically, the active input impedance can be computed for three scanning angles and 25 frequency points in less than a minute, while CST simulations take about three hours. Simulation have been performed on the same computer (workstation with six-core 3.20 GHz processor).

The performance achieved with the final design presented in this thesis are the following:

- The active reflection co-efficient for a single-pol array is from 7 to 14 GHz, whereas for a dual-pol array the -10 dB bandwidth is from 7 to 13 GHz.
- The array can scan up to 50° in all azimuthal planes.
- The radiation efficiency of the array is $> 95\%$.
- The maximum cross-pol level of the dual-pol array is -10 dB for scanning to 50° on the diagonal plane. This value is slightly higher than that obtained in the previous connected array designs (about -15 dB).

Although wider bandwidths are claimed in literature, e.g. in [33, 34], these performances are obtained accepting much lower efficiency in terms of matching (S_{11} lower than -6 dB). If we restrict the comparison with the state-of-the-art to high efficiency designs ($S_{11} < -10$ dB), the designs presented in this thesis are among the best reported for wide scanning and bandwidth performance. This improvement with respect to the previous solution is at the cost of slightly high cross-pol levels.

The proposed solution can be used for all the applications that require wideband and widescan performance. The applications includes multi-function radars, satellite communications and radioastronomy. The design presented in this thesis can be used as starting point for different designs, depending on the specific requirements of the considered application.

Possible extensions of this work include the combination of the analytical tool used for the analysis with an optimizer, for instance a generic algorithm, with the aim of achieving wider bandwidths or wider scanning angles. Moreover, recently dual-band designs are receiving increasing attention for radar applications, hence it is of interest to investigate the possibility of using the proposed solution for dual-band designs.

Bibliography

[1] K. Kegel and R. Bolt, "ACTiFE, Advanced Antenna Concepts for Aircraft in-Flight Entertainment, Identification antenna requirements," European Spase Agency, Noordwijk, Netherland, Tech. Rep. 3 WP 0300, ESA Contract no. C19865, May 2007.

[2] The SKA website. [Online]. Available: http://www.skatelescope.org/

[3] C. L. Carilli and S. Rawlings, Eds., *Science with the Square Kilometer Array.* New Astronomy Reviews, vol.48, Amsterdam: Elsevier, Dec. 2004.

[4] D. H. Schaubert, A. van Ardenne, and C. Craeye, "The Square Kilometer Array (SKA) antenna," in *Proc. IEEE Int. Symp. on Phased Array Systems and Technology*, Boston, MA, USA, Oct. 2003, pp. 351-358.

[5] Luca, De. "A new low-profile wide-scan phased array for UWB applications," *The Second European Conference on Antennas and Propogation, EuCAP 2007*, 2007.

[6] D. H. Schaubert, and T. H. Chio. "Wideband Vivaldi arrays for large aperture antennas," *Perspectives on Radio Astronomy: Technologies for Large Antenna Arrays.*, vol. 1, 2000.

[7] J. J. Lee, and S. Livingston. "Wide band bunny-ear radiating element." *Antennas and Propogation Society Internationsl Symposium, 1993. ap-s. Digest.* IEEE, 1993.

[8] Y. S. Kim and K. S. Yngvesson, "Characterization of tapered slot antenna feeds and feed arrays," *IEEE Trans. Antennas Propag.*, vol. 38, no. 10, Oct. 1990.

[9] D. Cavallo, "Connected Array Antennas: Analysis and Design," PhD. dissertation, Technische Universiteit Eindhoven, The Netherlands, 2011,

[10] W. H. Syed and A. Neto, "Front to back ratio enhancement of planar printed antennas by means of artificial dielectric layers," *IEEE Trans. Antennas Propag.*, vol. 61, no. 11, Nov. 2013.

[11] R. C. Hansen, "Linear connected arrays," *IEEE Antennas Wireless Propag. Lett.*, vol. 3, pp. 154-156, 2004.

[12] J.J. Lee, S. Livingstone, and R. Koenig, "Wide band slot array antennas," in *Proc. IEEE Antennas Propag. Symp.*, Columbus, OH, USA, Jun. 2003, vol. 2, pp. 452-455.

[13] J. J. Lee, S. Livingston, and D. Nagata, "A low profile 10:1 (200-2000 MHz) wide band long slot array," in *Proc. IEEE Antennas Propag. Int. Symp.*, San Diego, CA, USA, Jul. 5-11, 2008.

[14] J.J. Lee, S. Livingston, R. Koenig, D. Nagata, and L. L. Lai, "Compact light weight UHF arrays using long slot apertures," *IEEE Trans. Antennas Propag.*, vol. 54, no. 7, pp. 2009-2015, Jul. 2006.

[15] A. Neto and J. J. Lee, "Infinite bandwidth long slot array antenna," *IEEE Antennas Wireless Propag. Lett.*, vol 4, pp. 75-78, 2005.

[16] W. E. Kock, "Metallic delay lenses", *Bell Syst. Tech. J.*, vol. 27, no.1, pp.58-82, Jan. 1948.

[17] T. LaRocca, J. Y.-C. Liu, and M.-C. F. Chang, "60 GHz CMOS amplifiers using transformer-coupling and artificial dielectric differential transmission lines for compact design," *IEEE J. Solid-State Circuits*, vol. 44, no. 5, pp. 1425-1435, May 2009.

[18] S. C. Saha, J. P. Grant, Y. Ma, A. Khalid, F. Hong, and D. R. S. Cumming, "Terahertz frequency-domain spectroscopy method for vector characterization of liquid using an artificial dielectric," *IEEE Trans. THz Sci. Technol.*, vol. 2, no. 1, pp. 113-122, Jan. 2012.

[19] J. Zhang, P. A. R. Ade, P. Mauskopf, L. Moncelsi, G. Savini, and N. Whitehouse, "A new artificial dielectric metamaterial and its application

as a THz anti-reflection coating," *Appl. Opt.*, vol. 48, no. 35, pp. 6635-6642, Dec. 2009.

[20] K. Takahagi and, E. Sano, "High-gain silicon on-chip antenna with artificial dielectric layer," *IEEE Trans. Antennas Propag.*, vol.59, no.10, pp. 3624 - 3629, Oct. 2011.

[21] R. E. Collin, *Field Theory of Guided Waves, 2nd ed.* IEEE Press: New York, 1990, Ch. 12.

[22] D. Cavallo, W. H. Syed and A. Neto, "Closed-form analysis of artificial dielectric layers - Part I: properties of a single layer under plane-wave incidence," *IEEE Trans. Antennas Propag.*, submitted.

[23] D. Cavallo, W. H. Syed and A. Neto, "Closed-Form analysis of artificial dielectric layers - Part II: extension to multiple layers and arbitrary illumination," *IEEE Trans. Antennas Propag.*, submitted.

[24] M. A. Antoniades, "Microwave devices and antennas based on negative-refractive-index transmission-line metamaterials," *PhD dissertation.*, Univ. of Toronto, Canada.

[25] D. R. Smith, D. C. Vier, Th. Koschny, and C. M. Soukoulis,"Electromagnetic parameter retrieval from inhomogeneous metamaterials," *Physical Review E*, vol. 71, p. 036617, Mar. 2005.

[26] C. Menzel, C. Rockstuhl, T. Paul, F. Lederer, and T. Pertsch,"Retrieving effective parameters for metamaterials at oblique incidence," *Physical Review B*, vol. 77, p. 195328, May 2008.

[27] A. Hoofar, K. C. Gupta and D. C. Chang, "Cross-polarization level in radiation from a microstrip dipole antenna," *IEEE Trans. Antennas Propag.*, vol. 36, no. 9, pp. 1197-1203, Sep. 1988.

[28] D. M. Pozar, *Microwave Engineering, 3rd ed.* John & Wiley Sons, Inc., 2005, Ch. 5.

[29] M. Albani and F. Capolino, "Wave dynamics by a plane wave on a half-space metamaterial made of plasmonic nanospheres: a discrete Wiener Hopf formulation," *J. Opt. Soc. Am. B*, vol. 28, no. 9, pp. 2174-2185, Sep. 2011.

[30] D. Cavallo, A. Neto, and G. Gerini, “A 3 to 5 GHz prototype connected array of dipoles for wide-scanning, low X-pol applications," *IEEE Trans. Antennas Propag.*, vol. 28, no. 9, pp. 2174-2185, Sep. 2011..

[31] D. Cavallo,G. Gerini, R. Bolt, D. Deurloo, R. Grooters, A. Neto, G. Toso, and R. Midthassee , “Ku-band dual-polarized array of connected dipoles for satcom terminals: Theory and hardware validation,” *7th European Conference on Antenna and Propag.,* 2013.

[32] CST Microwave Studio 2011, [Online].Available: http://www.cst.com/.

[33] S. S. Holland and M. N. Vouvakis, “The planar ultrawideband modular antenna (PUMA) array," *IEEE Trans. Antennas Propag.*, vol. 60, no. 1, pp. 130-140, Jan. 2012.

[34] J. P. Doane, K. Sertel and J. L. Volakis, “A wideband, wide scanning tightly coupled dipole array with integrated balun (TCDA-IB)," *IEEE Trans. Antennas Propag.*, vol. 61, no. 9, pp. 4538-4548, Sep. 2013.